POLITECNICO DI TORINO
Repository ISTITUZIONALE

Coupling among deformation, fluid flow, structural reorganisation and fibre reorientation in fibre-reinforced, transversely isotropic biological tissues

Original
Coupling among deformation, fluid flow, structural reorganisation and fibre reorientation in fibre-reinforced, transversely isotropic biological tissues / Crevacore, Eleonora; Stefano, Salvatore Di; Grillo, Alfio. - In: INTERNATIONAL JOURNAL OF NON-LINEAR MECHANICS. - ISSN 0020-7462. - STAMPA. - 111:(2019), pp. 1-13. [10.1016/j.ijnonlinmec.2018.08.022]

Availability:
This version is available at: 11583/2722685 since: 2020-06-03T17:27:55Z

Publisher:
Elsevier

Published
DOI:10.1016/j.ijnonlinmec.2018.08.022

Terms of use:

This article is made available under terms and conditions as specified in the corresponding bibliographic description in the repository

Publisher copyright
Elsevier postprint/Author's Accepted Manuscript

© 2019. This manuscript version is made available under the CC-BY-NC-ND 4.0 license http://creativecommons.org/licenses/by-nc-nd/4.0/.The final authenticated version is available online at: http://dx.doi.org/10.1016/j.ijnonlinmec.2018.08.022

(Article begins on next page)

14 May 2024

Coupling among deformation, fluid flow, structural reorganisation and fibre reorientation in fibre-reinforced, transversely isotropic biological tissues

Eleonora Crevacore[a], Salvatore Di Stefano[a], Alfio Grillo[a,*]

[a] *Dipartimento di Scienze Matematiche (DISMA) "G.L. Lagrange"*
"Dipartimento di Eccellenza 2018–2022",
Politecnico di Torino, Corso Duca degli Abruzzi 24, 10129, Torino, Italy
E-mail: {eleonora.crevacore salvatore.distefano alfio.grillo}@polito.it

Abstract

We highlight some mechanical aspects of the coupling among deformation, fluid flow, structural evolution, and reorientation of fibres in fibre-reinforced, hydrated, soft biological tissues. For our purposes, we elaborate a model in which the tissue's interstitial fluid is inviscid and obeys Darcy's law, and the solid constituents are transversely isotropic, hyperelastic materials. Within this setting, we consider two different types of remodelling: One consists of the reorientation of the fibres, while the other one is the manifestation, at the tissue scale, of structural rearrangements representable in terms of inelastic distortions. Our focus is on the interplay between the latter ones and the fibre reorientation. In our model, such interplay is a consequence of the constitutive framework, which resolves explicitly the space variability of a parameter, the "fibre mean angle", that determines the direction along which the fibres tend to align themselves. Our main results concern the description of a Mandel-like stress tensor, which drives the inelastic distortions when the fibre mean angle is distributed inhomogeneously throughout the tissue, and of a diffusion-like tensor depending on the inelastic distortions, which guides the evolution of the fibre mean angle.

Keywords: Biological Tissues, Remodelling, Fibre Reorientation, Inelastic Distortions, Anisotropic Materials
2010 MSC: 74Bxx, 74Cxx, 74Fxx, 76Sxx, 76Zxx, 92Bxx

☆Submitted to the Special Issue "Multi-scale nonlinear continuum mechanical coupled field modelling and applications"

*Corresponding author
Email address: alfio.grillo@polito.it (Alfio Grillo)

1. Introduction

The study of fibre-reinforced composite materials is of great interest in Biomechanics, since it permits to understand various aspects of the mechanical behaviour of biological tissues. In the literature, there are works dedicated to fundamental questions, e.g. [1, 2, 3, 4], studies that infer the elastic and hydraulic properties of a tissue on the basis of micro-scale information, e.g. [5, 6, 7, 8, 9, 10, 11], and studies devoted to the formulation of computational methods and algorithms (see e.g. [12, 13, 14, 15, 16, 17]).

For fibre reinforced tissues, it is essential to provide a robust theoretical background to study their growth, structural reorganisation, and damage (see e.g. [18, 19, 20, 21, 22, 23]), and to relate such processes to the evolution of the material properties. This knowledge, indeed, is helpful for predicting the behaviour of injured or diseased tissues, and it may supply indications in the design of engineered tissues.

With these motivations, we propose to improve and extend the model presented in [24], where the reorientation of fibres was studied in a transversely isotropic fibre-reinforced tissue, with fibres aligned according to a prescribed probability density. Such probability density was parameterised by an angle denominated "fibre mean angle" and determining, at each material point, the direction of the most probable fibre alignment.

In the present work, there are three relevant differences with respect to [24]. The *first* and major difference is that we now account for plastic-like distortions and study their influence on the reorientation of the collagen fibres by adhering to the formalism introduced in [25]. Plastic-like distortions are meant to describe the onset and progression of irreversible strains in the tissue, which may arise in response to diseases or injuries [26], or the reorganisation of the tissue's extracellular matrix, as is the case for cellular aggregates and tumour spheroids [27, 28, 29]. In the literature, the concept of inelastic distortions is often related to that of residual stresses, an issue typically investigated with the aid of the Bilby-Kröner-Lee decomposition of the deformation gradient tensor. A rather different point view, however, has been recently proposed in [30], where a study on the impact of residual stresses on the mechanical behaviour of tissues is presented. The *second* difference is related to the rationale with which the concept of *target angle* is accounted for. We recall that the "target angle" is a preferred angle that, depending on the deformation or stress state in the tissue, contributes to direct the evolution of the fibre mean angle. In fact, it can be thought of as

the generator of an external force that drives the fibre mean angle towards the value determined by the interactions of the fibres with the environment in which they are embedded. After mentioning the approaches proposed, for example, in [12, 31, 32, 33], we select for our purposes a modification of the target angle put forward in [12]. The *third* difference is a re-definition of the constitutive framework and, in particular, of the free energy density of the Allen-Cahn type [24], which models the reorientation of the fibres and constituted the crux of [24] (see Sect. 4.2).

The most significant contribution of our work is the enrichment of the constitutive framework through the definition of two "non-standard" terms in the total free energy density of the system, W_ν. One of these terms, denoted by W_{Grad}, is said to be the "gradient part" of W_ν since it features the material gradient of the fibre mean angle, $\mathfrak{q}$. The energy density W_{Grad} keeps track, already at the constitutive level, of the *explicit* dependence of $\mathfrak{q}$ on material points [24]. Thus, such dependence is not inherited from the quantities involved in the evolution equation of $\mathfrak{q}$. Rather, it is accounted for *a priori* by enrolling $\mathrm{Grad}\mathfrak{q}$ among the constitutive arguments of W_ν. This gives rise to a generalised force that, by embodying the inhomogeneity of $\mathfrak{q}$, contributes to drive the evolution of $\mathfrak{q}$ itself. As a consequence, the coupling of $\mathfrak{q}$ with the dynamics of the plastic-like distortions introduce a novelty with respect to [24].

The other non-standard term in W_ν is referred to as the "structural part" and is denoted by W_{str}. In our view, it represents the potential energy that pertains to a given distribution of $\mathfrak{q}$, and its existence is postulated *a priori*, regardless of the fact that the tissue is deformed elastically or distorted inelastically. In fact, W_{str} can be non trivial also in the absence of deformation and plastic-like distortions, although we do allow for its coupling with these kinematic variables. The way in which this is done here is another novelty of our work, for we strongly modify the coupling previously defined in [24]. Moreover, we compare our concept of structural energy with the one introduced in [31], within a setting rather different from ours. This issue is addressed in Sect. 7.

The proposed constitutive framework leads to the key point of this work: The coupling among the kinematic variables is such that the dynamics of the system can be depicted as a "game among three players", i.e., the motion, the plastic-like distortions, and the fibre mean angle. The way in which they interact with one another is highlighted in Sect. 7.

In our model, plastic-like distortions are assumed to be set off, for in-

stance, when the tissue undergoes irreversible strains [26], when the cells of the tissue redistribute their adhesion bonds, or when the tissue's extracellular matrix rearranges the cross-links forming its structure [29]. In these cases, the solid constituent of the tissue experiences transformations that cannot be described in terms of shape changes, and that necessitate, thus, new descriptors. As suggested in [34], such descriptors should be regarded as independent kinematic variables that represent the structural degrees of freedom of the tissue. Within this picture, and by regarding the tissue as a deformable porous medium permeated by an interstitial fluid, our goal is to describe the interactions among deformation, fluid flow, and the aforementioned structural changes, emphasising the coupling between the plastic-like distortions and the fibre reorientation.

The remainder of this work is organised as follows. In Sect. 2 we enunciate the fundamental hypotheses of our model. In Sect. 3 we introduce all the model equations. In Sect. 4 we explain in detail the constitutive framework. In Sect. 5 we study the Dissipation Inequality. In Sect. 6 we comment on the results of our simulations. Finally, in Sect. 7 we present in detail our main theoretical achievements, and in Sect. 8 we summarise the key-points of our work, and we outline a possible future research.

2. Modelling hypotheses

We regard the tissue under study as a mixture comprising a solid and a fluid. The solid represents a porous medium and is assumed to feature a matrix and reinforcing collagen fibres. The matrix is composed of biological polymers and tissue cells. The fluid consists of water and several other chemical substances. In spite of its major role on the tissue's dynamics, in this study we neglect the presence of chemical substances other than water. On the one hand, this modelling choice precludes the resolution of the phenomena related to the tissue's chemistry. On the other hand, however, it is capable of accounting for a strong entanglement among the flow of the fluid, the deformation of the tissue, the reorganisation of its internal structure, and the reorientation of the reinforcing fibres, while containing computational costs. Moreover, the results predicted by our model can be used as inputs for studying the evolution of chemical agents, when the coupling between their dynamics and the aforementioned processes is weak enough.

The mathematical model discussed in this work rests on the following main hypotheses: (i) the solid is hyperelastic and the fluid macroscopically

inviscid; (ii) both constituents are intrinsically incompressible, so that the change of volume of the tissue as a whole is due to the variation of porosity (since the saturation condition applies, such variation is expressed through the variation of the volumetric fraction of the solid and of the fluid); (iii) the dynamics of the fluid adheres to Darcy's law; (iv) all body forces acting on the solid are negligible, with the exception of those describing the momentum exchange with the fluid; (v) growth is not accounted for in the model, so that the fluid and the solid locally preserve their mass.

3. Theoretical background

According to the hypotheses itemised above, the flow of the fluid and the deformation of the considered tissue are accounted for by the mass balance law and the linear momentum balance law for the tissue as a whole, i.e.,

$$\dot{J} = \mathrm{Div}\left[\boldsymbol{K}\,\mathrm{Grad}\,p\right], \qquad \text{in } \mathscr{B}\times\mathscr{I}, \tag{1a}$$

$$\mathrm{Div}\left[-Jp\,\boldsymbol{g}^{-1}\boldsymbol{F}^{-\mathrm{T}} + \boldsymbol{P}_{\mathrm{sc}}\right] = \boldsymbol{0}, \qquad \text{in } \mathscr{B}\times\mathscr{I}. \tag{1b}$$

In (1a) and (1b), $\boldsymbol{F}$ is the deformation gradient tensor of the solid, $J = \det\boldsymbol{F} > 0$ is said to be the *volume ratio*, p is the fluid pressure, $\boldsymbol{K}$ is referred to as the *material* permeability tensor of the tissue [9], $\boldsymbol{g}$ is the metric tensor associated with the three-dimensional Euclidean space $\mathscr{S}$, $\boldsymbol{P}_{\mathrm{sc}}$ is the constitutive part of the first Piola-Kirchhoff stress tensor of the solid, $\mathscr{B}\subset\mathscr{S}$ is a region of space that can be taken as reference for the considered solid-fluid mixture, and $\mathscr{I}$ is the interval of time over which the tissue is observed. We recall that $\boldsymbol{F}$ is the tangent map of the deformation $\chi:\mathscr{B}\times\mathscr{I}\to\mathscr{S}$ [35], which defines the configuration of the solid at time $t\in\mathscr{I}$, i.e., $\chi(\mathscr{B},t)=\mathscr{C}_{\mathrm{s}}(t)\in\mathscr{S}$ (see Appendix).

We first consider the reorganisation of the tissue due to the production of inelastic distortions. Since these are generally incompatible [34], i.e., they are not expressible as the gradient of a deformation, their descriptor should be at least a non-integrable second-order tensor field over $\mathscr{B}$. Following the same line of thought as Elastoplasticity, we indicate such tensor field by $\boldsymbol{F}_{\mathrm{p}}$, where the subscript "p" stands for "plastic-like distortions". Then, in accordance with [34], we introduce a set of generalised forces dual of the virtual velocity associated with $\boldsymbol{F}_{\mathrm{p}}$, and we distinguish between the internal and the external forces of this kind, denoted by $\boldsymbol{Y}_{\nu}^{\mathrm{int}}$ and $\boldsymbol{Y}_{\nu}^{\mathrm{ext}}$, respectively. Hence, by invoking

the Principle of Virtual Powers, we obtain the force balance [34]

$$\boldsymbol{Y}_{\nu}^{\mathrm{int}} = \boldsymbol{Y}_{\nu}^{\mathrm{ext}}, \quad \text{in } \mathscr{B} \times \mathscr{I}, \tag{2}$$

where the subscript "ν" means that $\boldsymbol{Y}_{\nu}^{\mathrm{int}}$ and $\boldsymbol{Y}_{\nu}^{\mathrm{ext}}$ are defined with respect to a relaxed state of the solid, which is said to be "natural state" [36]. Finally, using the jargon of [34], we remark that Eq. (2) is consistent with a "*grade zero*" theory, in which no gradient of $\boldsymbol{F}_{\mathrm{p}}$ is accounted for.

A rationale for $\boldsymbol{F}_{\mathrm{p}}$ is provided by the Bilby-Kröner-Lee (BKL) multiplicative decomposition of $\boldsymbol{F}$ (see [37] for a review), i.e., $\boldsymbol{F} = \boldsymbol{F}_{\mathrm{e}}\boldsymbol{F}_{\mathrm{p}}$, where $\boldsymbol{F}_{\mathrm{e}}$ is said to be the tensor of elastic distortions. For every $X \in \mathscr{B}$ and $t \in \mathscr{I}$, we set $\boldsymbol{F}_{\mathrm{p}}(X,t) : T_X\mathscr{B} \to \mathscr{N}_t(X)$ and $\boldsymbol{F}_{\mathrm{e}}(X,t) : \mathscr{N}_t(X) \to T_{\chi(X,t)}\mathscr{S}$, where $T_X\mathscr{B}$ is the tangent space attached to $X \in \mathscr{B}$, $\mathscr{N}_t(X)$ is the image of $T_X\mathscr{B}$ through $\boldsymbol{F}_{\mathrm{p}}(X,t)$ [38], and $T_{\chi(X,t)}\mathscr{S}$ is the tangent space of $\mathscr{S}$ in $x = \chi(X,t)$. For future use, we also introduce the tangent bundles $T\mathscr{B} = \sqcup_{X\in\mathscr{B}} T_X\mathscr{B}$ and $T\mathscr{S} = \sqcup_{x\in\mathscr{S}} T_x\mathscr{S}$ associated with $\mathscr{B}$ and $\mathscr{S}$, respectively. Note that we adopt the letter "$\mathscr{N}$" in $\mathscr{N}_t(X)$ in order to highlight that the vectors of $\mathscr{N}_t(X)$ are in the natural state, i.e., they are relaxed. Accordingly, $\mathscr{N}_t(X)$ describes a stress-free state of the material at X, as depicted in Fig. 1 (note that the above notation has been recently used in [39]).

We denote by $\boldsymbol{g}$ and $\boldsymbol{G}$ the metric tensors associated with $\mathscr{S}$ and $\mathscr{B}$, respectively, so that the Cauchy-Green deformation tensor, $\boldsymbol{C} = \boldsymbol{F}^{\mathrm{T}}.\boldsymbol{F} = \boldsymbol{F}^{\mathrm{T}}\boldsymbol{g}\boldsymbol{F}$, reduces to $\boldsymbol{C} = \boldsymbol{G}$ in the absence of deformation [35]. In addition, we introduce the metric tensor $\boldsymbol{\eta}$, associated with the tissue's natural state, which allows to define the tensors $\boldsymbol{C}_{\mathrm{p}} = \boldsymbol{F}_{\mathrm{p}}^{\mathrm{T}}.\boldsymbol{F}_{\mathrm{p}} = \boldsymbol{F}_{\mathrm{p}}^{\mathrm{T}}\boldsymbol{\eta}\boldsymbol{F}_{\mathrm{p}}$ and $\boldsymbol{B}_{\mathrm{p}} = \boldsymbol{C}_{\mathrm{p}}^{-1} = \boldsymbol{F}_{\mathrm{p}}^{-1}\boldsymbol{\eta}^{-1}\boldsymbol{F}_{\mathrm{p}}^{-\mathrm{T}}$. We keep $\boldsymbol{\eta}$ formally different from $\boldsymbol{g}$ and $\boldsymbol{G}$, although, in some cases, it could be taken equal to one of those (see e.g. [33]). For future use, we also define the right elastic Cauchy-Green tensor $\boldsymbol{C}_{\mathrm{e}} = \boldsymbol{F}_{\mathrm{e}}^{\mathrm{T}}.\boldsymbol{F}_{\mathrm{e}} = \boldsymbol{F}_{\mathrm{e}}^{\mathrm{T}}\boldsymbol{g}\boldsymbol{F}_{\mathrm{e}}$.

We now turn to the reorientation of the reinforcing fibres. As reported in [31, 24, 40], the alignment of the fibres in the tissue is governed by a probability density that depends on a given set of scalar parameters. The variation of these parameters is responsible for the reorientation of the fibres. In our model (see Sect. 4), we select one parameter only, which we indicate with $\mathfrak{q}$ and employ to describe the kinematics of the fibres. In particular, $\mathfrak{q}$ acquires the meaning of "fibre mean angle". Analogously to the reasoning that has led us to (2), we consider both internal and external generalised forces dual of the (scalar) virtual velocity $\mathfrak{v}$ associated with $\mathfrak{q}$. In this case, however, since we aim at resolving explicitly the point dependence of $\mathfrak{q}$,

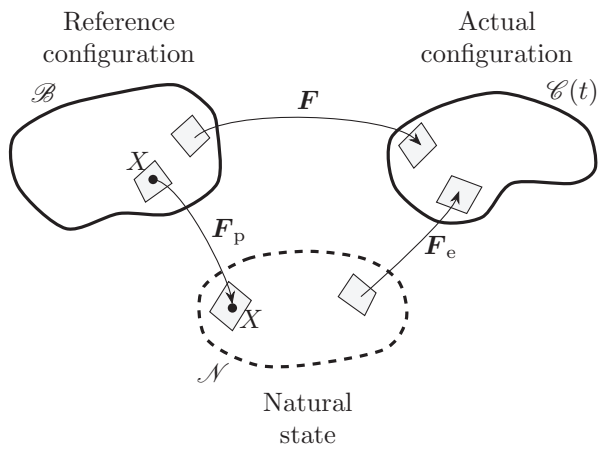

Figure 1: Graphical representation of the Bilby-Kröner-Lee (BKL) multiplicative decomposition of the deformation gradient tensor $\boldsymbol{F}$, i.e., $\boldsymbol{F} = \boldsymbol{F}_{\mathrm{e}}\boldsymbol{F}_{\mathrm{p}}$

we also need to account for the kinematic descriptor $\operatorname{Grad}\mathfrak{q}$, along with its virtual counterpart $\operatorname{Grad}\mathfrak{v}$. Then, by employing again the Principle of Virtual Powers, and restricting it for brevity only to the sub-problem of the fibre reorientation, we find

$$\int_{\mathscr{B}} \left\{ y^{(0)}\mathfrak{v} + \boldsymbol{y}^{(1)} \operatorname{Grad}\mathfrak{v} \right\} = \int_{\mathscr{B}} h^{(0)}\mathfrak{v} + \int_{\partial\mathscr{B}_N} h^{(1)}\,\mathfrak{v}, \tag{3}$$

where $y^{(0)}$ and $\boldsymbol{y}^{(1)}$ are a scalar and a vector-like internal force, defined as the dual entities of $\mathfrak{v}$ and $\operatorname{Grad}\mathfrak{v}$, respectively, $h^{(0)}$ is an external force, $h^{(1)}$ is an external contact force, $\partial\mathscr{B}_N$ is the Neumann boundary of $\partial\mathscr{B}$, and the virtual velocity $\mathfrak{v}$ is assumed to vanish identically on the Dirichlet portion of $\partial\mathscr{B}$, i.e., on $\partial\mathscr{B}_D = \partial\mathscr{B}\backslash\partial\mathscr{B}_N$. Equation (3) leads to the balance laws

$$y^{(0)} - \operatorname{Div}\boldsymbol{y}^{(1)} = h^{(0)}, \qquad \text{in } \mathscr{B}\times\mathscr{I}, \tag{4a}$$

$$\boldsymbol{y}^{(1)}.\boldsymbol{N} = h^{(1)}, \qquad \text{on } \partial\mathscr{B}_N\times\mathscr{I}. \tag{4b}$$

Upon setting, in the case of isochoric plastic-like distortions,

$$\mathscr{R}_{\nu}^{\mathrm{ext}} \equiv h^{(0)}, \tag{5a}$$

$$\mathscr{R}_{\nu}^{\mathrm{int}} \equiv y^{(0)} - \operatorname{Div}\boldsymbol{y}^{(1)}, \tag{5b}$$

we can rephrase (4a) as

$$\mathscr{R}_\nu^{\text{int}} = \mathscr{R}_\nu^{\text{ext}}, \quad \text{in } \mathscr{B} \times \mathscr{I}, \tag{6}$$

thereby generalising the results in [33, 40]. Equations (1a), (1b), (2), reformulated for the case of isochoric plastic-like distsortions, and (6) describe the dynamics of the system under study. Their solution determines the model unknowns, identified with p, χ, $\boldsymbol{F}_{\text{p}}$, and $\mathfrak{q}$. Among those, a *true* configuration of the solid is obtained by specifying the triple of descriptors $(\chi, \boldsymbol{F}_{\text{p}}, \mathfrak{q})$. In the sequel, we refer to $\mathfrak{q}$ and $\boldsymbol{F}_{\text{p}}$ as to *remodelling variables*, and to $\boldsymbol{Y}_\nu^{\text{int}}$, $\boldsymbol{Y}_\nu^{\text{ext}}$, $\mathscr{R}_\nu^{\text{int}}$, and $\mathscr{R}_\nu^{\text{ext}}$ as to generalised *remodelling forces*.

4. Constitutive laws

To constitutively characterise the fibre-reinforced medium under study, we assign a free energy density consisting of two terms, both of which are written per unit volume of the material in its natural state, i.e. [24],

$$W_\nu = W_{\text{std}} + W_{\text{rem}}. \tag{7}$$

The term W_{std} takes into account the hyperelastic behaviour of the solid material, and relies on a mechanical model of fibre-reinforced media, in which the fibres are oriented statistically [6, 7, 9]. In this respect, we denote the corresponding strain energy density by W_{std}, where the subscript "std" stands for "standard". The other term, W_{rem}, is not standard and it has been introduced in order to specifically account for remodelling [31, 24, 41]. The energy density W_{rem} is assumed to exist independently of deformation and, in fact, it is conceived as the energetic contribution that characterises each possible directional distribution of the fibres in the tissue. For this reason, W_{rem} may be nontrivial also in the undeformed configuration of the tissue [24].

4.1. "Standard" Constitutive laws

Following [6, 7, 9, 24, 40], we define W_{std} as a function of $\boldsymbol{C}_{\text{e}}$ and $\mathfrak{q}$, i.e., we set $W_{\text{std}} = \hat{W}_{\text{std}}(\boldsymbol{C}_{\text{e}}, \mathfrak{q})$, with

$$\hat{W}_{\text{std}}(\boldsymbol{C}_{\text{e}}, \mathfrak{q}) = \Phi_{\text{s}\nu}\hat{U}(J_{\text{e}}) + \Phi_{0\text{s}\nu}\hat{W}_0(\boldsymbol{C}_{\text{e}}) + \Phi_{1\text{s}\nu}\left[\hat{W}_{1\text{i}}(\boldsymbol{C}_{\text{e}}) + \hat{W}_{1\text{a}}(\boldsymbol{C}_{\text{e}}, \mathfrak{q})\right]. \tag{8}$$

In (8), $\Phi_{\mathrm{s}\nu} = J_{\mathrm{e}}\phi_{\mathrm{s}}$, $\Phi_{0\mathrm{s}\nu} = J_{\mathrm{e}}\phi_{0\mathrm{s}}$, and $\Phi_{1\mathrm{s}\nu} = J_{\mathrm{e}}\phi_{1\mathrm{s}}$ are the volumetric fractions of the solid as a whole, of the matrix, and of the fibres, respectively, all expressed per unit volume of the solid in the natural state, and $J_{\mathrm{e}} = \sqrt{\det \boldsymbol{C}_{\mathrm{e}}}$ is the volume ratio associated with the elastic distortions; $\hat{U}(J_{\mathrm{e}})$ is a *penalty* term, introduced to prevent the tissue from the occurrence of compaction [9, 42]; $\hat{W}_0(\boldsymbol{C}_{\mathrm{e}})$ is the strain energy density of the solid matrix, assumed to be isotropic; $\hat{W}_{1\mathrm{i}}(\boldsymbol{C}_{\mathrm{e}})$ and $\hat{W}_{1\mathrm{a}}(\boldsymbol{C}_{\mathrm{e}}, \mathfrak{q})$ are the *isotropic* and the *anisotropic* strain energy densities of the fibres, respectively. The latter one is defined through the directional average [3, 7, 9, 14, 43, 44]

$$\hat{W}_{1\mathrm{a}}(\boldsymbol{C}_{\mathrm{e}}, \mathfrak{q}) = \left\langle\!\!\left\langle \hat{\mathscr{W}}_{1\mathrm{a}}(\boldsymbol{C}_{\mathrm{e}}, \mathbf{m}) \right\rangle\!\!\right\rangle (\mathfrak{q}), \tag{9}$$

where $\langle\!\langle \bullet \rangle\!\rangle$ is the operator of directional averaging, $\hat{\mathscr{W}}_{1\mathrm{a}}(\boldsymbol{C}_{\mathrm{e}}, \mathbf{m})$ is the transversely isotropic strain energy density of a single fibre, and $\mathbf{m}$ is a field of unit vectors individuating the direction of space along which the fibres are locally oriented.

Possible explicit constitutive expressions for $\hat{U}(J_{\mathrm{e}})$, $\hat{W}_0(\boldsymbol{C}_{\mathrm{e}})$, $\hat{W}_{1\mathrm{i}}(\boldsymbol{C}_{\mathrm{e}})$, and $\hat{\mathscr{W}}_{1\mathrm{a}}(\boldsymbol{C}_{\mathrm{e}}, \mathbf{m})$ are given by [9, 45]

$$\hat{U}(J_{\mathrm{e}}) = \alpha_0 \frac{[J_{\mathrm{e}} - J_{\mathrm{cr}}]^{2q}}{[J_{\mathrm{e}} - \Phi_{\mathrm{s}\nu}]^{r}} \mathcal{H}(J_{\mathrm{cr}} - J_{\mathrm{e}}), \tag{10a}$$

$$\begin{aligned} \hat{W}_0(\boldsymbol{C}_{\mathrm{e}}) &= \check{W}_0(I_{1\mathrm{e}}, I_{2\mathrm{e}}, I_{3\mathrm{e}}) \\ &= \alpha_0 \left\{ \frac{\exp\left(\alpha_1[I_{1\mathrm{e}} - 3] + \alpha_2[I_{2\mathrm{e}} - 3]\right)}{I_{3\mathrm{e}}^{\alpha_3}} - 1 \right\}, \end{aligned} \tag{10b}$$

$$\begin{aligned} \hat{W}_{1\mathrm{i}}(\boldsymbol{C}_{\mathrm{e}}) &= \check{W}_{1\mathrm{i}}(I_{1\mathrm{e}}, I_{2\mathrm{e}}, I_{3\mathrm{e}}) \\ &= \alpha_{\mathrm{i}0} \left\{ \frac{\exp\left(\alpha_{\mathrm{i}1}[I_{1\mathrm{e}} - 3] + \alpha_{\mathrm{i}2}[I_{2\mathrm{e}} - 3]\right)}{I_{3\mathrm{e}}^{\alpha_{\mathrm{i}3}}} - 1 \right\}, \end{aligned} \tag{10c}$$

$$\hat{\mathscr{W}}_{1\mathrm{a}}(\boldsymbol{C}_{\mathrm{e}}, \mathbf{m}) = \check{\mathscr{W}}_{1\mathrm{a}}(I_{4\mathrm{e}}) = \check{\mathscr{V}}_{1\mathrm{a}}(I_{4\mathrm{e}})\mathcal{H}(I_{4\mathrm{e}} - 1), \tag{10d}$$

$$\check{\mathscr{V}}_{1\mathrm{a}}(I_{4\mathrm{e}}) = \frac{k_1}{2k_2} \left\{ \exp\left(k_2[I_{4\mathrm{e}} - 1]^2\right) - 1 \right\}. \tag{10e}$$

The constitutive expression of $\check{\mathscr{V}}_{1\mathrm{a}}$ is taken from [33, 46]. We remark that, although we are aware of the importance of the invariant $I_{5\mathrm{e}} = \boldsymbol{C}_{\mathrm{e}}^2 : (\mathbf{m} \otimes \mathbf{m})$ in the formulation of the anisotropic part of the strain energy density (see e.g. [47, 48]), we retained here the form (10d) of $\hat{\mathscr{W}}_{1\mathrm{a}}(\boldsymbol{C}_{\mathrm{e}}, \mathbf{m})$ because, since it has been used in other works, it allows us for an easier comparison with

the results obtained in the presence of remodelling.

In (10a)–(10d), $I_{1\mathrm{e}} = \mathrm{tr}(\boldsymbol{C}_\mathrm{e})$, $I_{2\mathrm{e}} = \frac{1}{2}[I_{1\mathrm{e}}^2 - \mathrm{tr}(\boldsymbol{C}_\mathrm{e}^2)]$, and $I_{3\mathrm{e}} = J_\mathrm{e}^2 = \det \boldsymbol{C}_\mathrm{e}$ are the principal invariants of $\boldsymbol{C}_\mathrm{e}$, $I_{4\mathrm{e}}$ is given by $I_{4\mathrm{e}} = \boldsymbol{C}_\mathrm{e} : (\mathfrak{m} \otimes \mathfrak{m})$, $\mathcal{H}(I_{4\mathrm{e}} - 1)$ is the Heaviside function, J_cr is a critical value of J_e below which $\hat{U}(J_\mathrm{e})$ is active (see [9] for details), and $\{\alpha_0, \alpha_1, \alpha_2\}$, $\{\alpha_{\mathrm{i}0}, \alpha_{\mathrm{i}1}, \alpha_{\mathrm{i}2}\}$, and $\{k_1, k_2\}$ are sets of material parameters (see Table 1). In particular, α_0, $\alpha_{\mathrm{i}0}$ and k_1 have physical units of energy per unit volume. As prescribed in [41], we enforce the conditions $\alpha_3 = \alpha_1 + 2\alpha_2$ and $\alpha_{\mathrm{i}3} = \alpha_{\mathrm{i}1} + 2\alpha_{\mathrm{i}2}$. By attaching the *set of all space directions*

$$\mathbb{S}^2_X \mathscr{B} = \{\mathfrak{m}_X : \ \|\mathfrak{m}_X\| = 1\} \tag{11}$$

to each $X \in \mathscr{B}$, and by defining the bundle $\mathbb{S}^2\mathscr{B} = \sqcup_{X \in \mathscr{B}} \mathbb{S}^2_X \mathscr{B}$, the field of unit vectors $\mathfrak{m}$ can be re-defined as $\mathfrak{m} : \mathscr{B} \to \mathbb{S}^2\mathscr{B}$, so that $\mathfrak{m}(X) = \mathfrak{m}_X \in \mathbb{S}^2_X \mathscr{B}$. Finally, the directional average (9),

$$\hat{W}_{1\mathrm{a}}(\boldsymbol{C}_\mathrm{e}, \mathfrak{q}) = \left\langle\!\!\left\langle \hat{\mathscr{W}}_{1\mathrm{a}}(\boldsymbol{C}_\mathrm{e}, \mathfrak{m}) \right\rangle\!\!\right\rangle (\mathfrak{q}) := \int_{\mathbb{S}^2\mathscr{B}} \hat{\mathscr{W}}_{1\mathrm{a}}(\boldsymbol{C}_\mathrm{e}, \mathfrak{m}) \Psi(\mathfrak{m}, \mathfrak{q}), \tag{12}$$

is computed with respect to a given probability density Ψ (see e.g. [7, 3, 14]). Here, Ψ is assumed to depend only on the direction of the local fibre orientation and on the remodelling variable, $\mathfrak{q}$. However, in more general contexts, it can depend on several other parameters. It is important to remark that, in this work, it is taken transversely isotropic with respect to a direction $\mathfrak{m}_0$ for the tissue as a whole. To justify this assumption, we consider a specimen of tissue of cylindric shape, and we assume that the symmetry axis of the cylinder coincides with $\mathfrak{m}_0$.

We remark that $\hat{\mathscr{W}}_{1\mathrm{a}}(\boldsymbol{C}_\mathrm{e}, \mathfrak{m})$ depends on $\mathfrak{m}$ through the structure tensor $\mathfrak{a} := \mathfrak{m} \otimes \mathfrak{m}$ and, since $\mathfrak{a}$ is invariant under the transformation $\mathfrak{m} \mapsto -\mathfrak{m}$, it also holds that $\hat{\mathscr{W}}_{1\mathrm{a}}(\boldsymbol{C}_\mathrm{e}(X,t), \mathfrak{m}_X) = \hat{\mathscr{W}}_{1\mathrm{a}}(\boldsymbol{C}_\mathrm{e}(X,t), -\mathfrak{m}_X)$, for all $X \in \mathscr{B}$ and for all times.

While the strain energy density of a single fibre, $\hat{\mathscr{W}}_{1\mathrm{a}}(\boldsymbol{C}_\mathrm{e}, \mathfrak{m})$, is transversely isotropic with respect to $\mathfrak{m}$, the directional average (9) models a material that is transversely isotropic with respect to $\mathfrak{m}_0$. To guarantee this property, for all $X \in \mathscr{B}$ in the natural state, we first choose a triad $\{\mathfrak{e}_\alpha(X)\}_{\alpha=1}^3$ of basis unit vectors, with $\mathfrak{e}_3(X)$ parallel to $\mathfrak{m}_0$. Then, we introduce the polar coordinates $(\vartheta, \varphi) \in [0, \pi] \times [0, 2\pi[$, so that $\mathfrak{m}_X$ reads

$$\mathfrak{m}_X \equiv \check{\mathfrak{m}}_X(\vartheta, \varphi) = \sin\vartheta \, \cos\varphi \, \mathfrak{e}_1 + \sin\vartheta \, \sin\varphi \, \mathfrak{e}_2 + \cos\vartheta \, \mathfrak{e}_3, \tag{13}$$

Symbol	Definition	Units	Symbol	Definition	Units
r	0.50	[—]	$\Phi_{0s\nu}$	$0.046 + 0.038\xi - 0.062\xi^2$	[—]
q	2.00	[—]	$\Phi_{1s\nu}$	$0.204 - 0.138\xi + 0.062\xi^2$	[—]
α_0	0.125	[MPa]	Γ	$1 \cdot 10^4$	[Pa s]
$\alpha_1 = \alpha_{i1}$	0.778	[—]	D_0	$1 \cdot 10^{-4}$	$[\mathrm{N(rad)}^{-1}]$
$\alpha_2 = \alpha_{i2}$	0.111	[—]	ζ_0	0.50	$[(\mathrm{MPa\ s})^{-1}]$
α_{i0}	7.59	[MPa]	e_ν	$(1 - \Phi_{s\nu})/\Phi_{s\nu}$	[—]
J_{cr}	$0.1 + \Phi_{s\nu}(\xi)$	[—]	$e_\nu^{(0)}$	4.0	[—]
k_1	13.00	[kPa]	κ_0	0.0848	[—]
k_2	12.20	[—]	m_0	4.6380	[—]
σ_y	0.002	[MPa]	$k_{0\nu}^{(0)}$	$3.7729 \cdot 10^{-3}$	$[\mathrm{mm}^4(\mathrm{N\ s})^{-1}]$
$\Phi_{s\nu}$	$\Phi_{0s\nu} + \Phi_{1s\nu}$	[—]	$\mathscr{A}_0$	$(k_1/k_2)(4.387\,\xi^{2.228} + 1)$	[kPa]

Table 1: Parameters used in the energy densities (10a)–(10e). See [9, 45], and the references therein, for the values in the first seven rows on the left. Note that $\xi = \frac{X^3}{L}$.

and we enforce the condition

$$\Psi(\mathbf{m}_X, \mathfrak{q}) = \Psi(\check{\mathbf{m}}_X(\vartheta, \varphi), \mathfrak{q}) \equiv \check{\Psi}(\vartheta, \mathfrak{q}). \tag{14}$$

Since the probability density $\check{\Psi}(\vartheta, \mathfrak{q})$ re-defined in (14) is independent of φ, the directional average (9) has to be transversely isotropic with respect to $\mathbf{m}_0$. Several functional forms can be used to express $\check{\Psi}(\vartheta, \mathfrak{q})$. For example, it can be a pseudo-Gaussian distribution [31, 24, 40, 49], defined by

$$\check{\Psi}_{\mathrm{PG}}(\vartheta, \mathfrak{q}) \equiv \hat{\Psi}_{\mathrm{PG}}(\vartheta, \mathfrak{q}, \omega) = \frac{\hat{\gamma}(\vartheta, \mathfrak{q}, \omega)}{\mathcal{N}(\mathfrak{q}, \omega)}, \tag{15a}$$

$$\hat{\gamma}(\vartheta, \mathfrak{q}, \omega) = \exp\left(-\frac{(\vartheta - \mathfrak{q})^2}{2\omega^2}\right), \tag{15b}$$

$$\mathcal{N}(\mathfrak{q}, \omega) = 2\pi \int_0^{\pi/2} \hat{\gamma}(\vartheta, \mathfrak{q}, \omega) \sin\vartheta \, \mathrm{d}\vartheta. \tag{15c}$$

In (15a)–(15c), $\omega^2 > 0$ is the variance of the pseudo-Gaussian distribution, $\mathcal{N}(\mathfrak{q}, \omega)$ is the normalisation factor, and the remodelling angle $\mathfrak{q}$ is the angle, taken from $\mathbf{m}_0$, that denotes the semi-aperture of a cone of fibres with the apex in X. The angle $\mathfrak{q}$ is conceived in such a way that $\check{\mathbf{m}}(\mathfrak{q}, \varphi)$ represents the set of most probable directions of fibre alignement, with φ varying in

$\in [0, 2\pi[$. We remark that, according to the definitions (15a)–(15c), the values of ϑ that are admissible for $\check{\Psi}_{\rm PG}$ range in $[0, \pi/2]$. For this reason, also $\mathfrak{q}$ is allowed to vary within the same interval only.

Other forms of the probability density can be found e.g. in [31, 44]

4.2. "Non-Standard" constitutive laws

The energy density associated with remodelling is given in the form [24]

$$\hat{W}_{\rm rem}(\boldsymbol{F}_{\rm e}, \boldsymbol{F}_{\rm p}, \mathfrak{q}, {\rm Grad}\,\mathfrak{q}) = \Phi_{1s\nu}\left[\hat{W}_{\rm str}(\boldsymbol{C}_{\rm e}, \mathfrak{q}) + \hat{W}_{\rm Grad}(\boldsymbol{F}_{\rm e}, \boldsymbol{F}_{\rm p}, {\rm Grad}\,\mathfrak{q})\right], \quad (16)$$

where $\hat{W}_{\rm str}(\boldsymbol{C}_{\rm e}, \mathfrak{q})$ and $\hat{W}_{\rm Grad}(\boldsymbol{F}_{\rm e}, \boldsymbol{F}_{\rm p}, {\rm Grad}\,\mathfrak{q})$ are referred to as the *structural* part and the *gradient* part of the strain energy density, respectively. Although (16) has recently been introduced in [24], in the present work the constitutive expressions of $\hat{W}_{\rm str}$ and $\hat{W}_{\rm Grad}$ are rather different from those supplied in [24].

The first difference concerns $\hat{W}_{\rm str}(\boldsymbol{C}_{\rm e}, \mathfrak{q})$, which is assumed here to be transversely isotropic, and to depend on $\boldsymbol{C}_{\rm e}$ only through $\bar{\boldsymbol{C}}_{\rm e} = J_{\rm e}^{-2/3}\boldsymbol{C}_{\rm e}$, i.e.,

$$\hat{W}_{\rm str}(\boldsymbol{C}_{\rm e}, \mathfrak{q}) = \mathscr{A}_0 \mathscr{P}(\mathfrak{q})\left[1 + \frac{k_2}{k_1}\left\langle\!\!\left\langle \check{\mathscr{V}}_{1\rm a}(\bar{I}_{4\rm e})\mathcal{H}(I_{4\rm e} - 1)\right\rangle\!\!\right\rangle(\mathfrak{q})\right], \quad (17)$$

where $\bar{I}_{4\rm e} = \bar{\boldsymbol{C}}_{\rm e} : (\mathfrak{m} \otimes \mathfrak{m}) = J_{\rm e}^{-2/3} I_{4\rm e}$, $\mathscr{A}_0$ is a point-dependent material coefficient, and $\mathscr{P}(\mathfrak{q})$ a double-well function of the fibre mean angle [24], i.e.,

$$\mathscr{P}(\mathfrak{q}) = \frac{1}{(\pi/4)^4}\mathfrak{q}^2\left(\mathfrak{q} - \frac{\pi}{2}\right)^2. \quad (18)$$

As noticed above, a more complete constitutive approach would call for expressing $\check{\mathscr{V}}_{1\rm a}$ as a function of both $I_{4\rm e}$ and $I_{5\rm e}$ [47]. However, since such a modelling choice does not change the "philosophy" of our work, we opt here for an easier form of $\check{\mathscr{V}}_{1\rm a}$.

The second difference concerns the definition of $W_{\rm Grad}$, which is assumed to depend also on the plastic-like distortions through the expression

$$\begin{aligned} W_{\rm Grad} &= \tfrac{1}{2}\boldsymbol{d} : {\rm grad}^{\rm s}\mathfrak{q} \otimes {\rm grad}^{\rm s}\mathfrak{q} \\ &= \tfrac{1}{2}\boldsymbol{F}_{\rm p}^{-1}\boldsymbol{F}_{\rm e}^{-1}\boldsymbol{d}\boldsymbol{F}_{\rm e}^{-\rm T}\boldsymbol{F}_{\rm p}^{-\rm T} : {\rm Grad}\,\mathfrak{q} \otimes {\rm Grad}\,\mathfrak{q}, \end{aligned} \quad (19)$$

where we employed the identity ${\rm grad}^{\rm s}\mathfrak{q}(x,t) = \boldsymbol{F}^{-\rm T}(X,t){\rm Grad}\,\mathfrak{q}(X,t)$, with

${}^{\mathrm{s}}\mathfrak{q}(\,\cdot\,,t) : \mathscr{C}(t) \to [0,\pi/2]$ being the spatial version of the fibre mean angle. Among the many possible choices for expressing the second-order tensor $\boldsymbol{d}$, which has the physical meaning of angular stiffness per unit length [24], we select $\boldsymbol{d} = D_0\boldsymbol{b}_{\mathrm{e}}$, where $\boldsymbol{b}_{\mathrm{e}} = \boldsymbol{F}_{\mathrm{e}}.\boldsymbol{F}_{\mathrm{e}}^{\mathrm{T}}$ is the elastic left Cauchy-Green deformation tensor, and the coefficient D_0 is assumed to be constant. In general, D_0 should be a function of material points. However, in this work, we attribute the dependence on material points to the "effective" coefficient $\Phi_{1\mathrm{s}\nu}D_0$, which features in the definition of W_{rem}, and is obtained by multiplying W_{Grad} by $\Phi_{1\mathrm{s}\nu}$, as done in (16). Upon substituting $\boldsymbol{d} = D_0\boldsymbol{b}_{\mathrm{e}}$ into (19), we can rephrase W_{Grad} as a function of $\boldsymbol{F}_{\mathrm{p}}$ and $\mathrm{Grad}\,\mathfrak{q}$, i.e.,

$$W_{\mathrm{Grad}} = \tilde{W}_{\mathrm{Grad}}(\boldsymbol{F}_{\mathrm{p}}, \mathrm{Grad}\,\mathfrak{q}) = \tfrac{1}{2}D_0\boldsymbol{B}_{\mathrm{p}} : \mathrm{Grad}\,\mathfrak{q} \otimes \mathrm{Grad}\,\mathfrak{q}. \tag{20}$$

5. Residual Dissipation Inequality and Remodelling Equations

We adapt the study of the dissipation inequality from [24, 50] and, to avoid lengthy calculations, we report here only the results that are most important for this work. By exploiting the identity $\boldsymbol{C}_{\mathrm{e}} = \boldsymbol{F}_{\mathrm{p}}^{-\mathrm{T}}\boldsymbol{C}\boldsymbol{F}_{\mathrm{p}}^{-1}$, we can rephrase the constitutive expression of the overall free energy density W_ν (see Sect. 4) as a function of $\boldsymbol{C}$, $\boldsymbol{F}_{\mathrm{p}}$ and $\mathfrak{q}$, i.e.,

$$W_\nu = \tilde{W}_\nu(\boldsymbol{C}, \boldsymbol{F}_{\mathrm{p}}, \mathfrak{q}, \mathrm{Grad}\,\mathfrak{q}). \tag{21}$$

By assuming isochoric plastic-like distortions, i.e., $J_{\mathrm{p}} = 1$, we obtain

$$\boldsymbol{P}_{\mathrm{s}} = -\Phi_{\mathrm{s}\nu}p\,\boldsymbol{g}^{-1}\boldsymbol{F}^{-\mathrm{T}} + \boldsymbol{F}\left(2\frac{\partial\tilde{W}_\nu}{\partial\boldsymbol{C}}\right), \tag{22a}$$

$$\boldsymbol{P}_{\mathrm{f}} = -(J - \Phi_{\mathrm{s}\nu})p\,\boldsymbol{g}^{-1}\boldsymbol{F}^{-\mathrm{T}}, \tag{22b}$$

where $\boldsymbol{P}_{\mathrm{s}}$ and $\boldsymbol{P}_{\mathrm{f}}$ are the first Piola-Kirchhoff stress tensors of the solid and the fluid, respectively. Next, we write $W_{\mathrm{std}} = \tilde{W}_{\mathrm{std}}(\boldsymbol{C}, \boldsymbol{F}_{\mathrm{p}}, \mathfrak{q})$, $W_{\mathrm{str}} = \tilde{W}_{\mathrm{str}}(\boldsymbol{C}, \boldsymbol{F}_{\mathrm{p}}, \mathfrak{q})$, and $W_{\mathrm{Grad}} = \tilde{W}_{\mathrm{Grad}}(\boldsymbol{F}_{\mathrm{p}}, \mathrm{Grad}\mathfrak{q})$. Subsequently, we introduce the Mandel stress tensors

$$\boldsymbol{\Sigma}_{\mathrm{std}} = -\boldsymbol{F}_{\mathrm{p}}^{\mathrm{T}}\frac{\partial\tilde{W}_{\mathrm{std}}}{\partial\boldsymbol{F}_{\mathrm{p}}} = \boldsymbol{C}\left(2\frac{\partial\tilde{W}_{\mathrm{std}}}{\partial\boldsymbol{C}}\right), \tag{23a}$$

$$\boldsymbol{\Sigma}_{\mathrm{str}} = -\boldsymbol{F}_{\mathrm{p}}^{\mathrm{T}}\left(\Phi_{1\mathrm{s}\nu}\frac{\partial \tilde{W}_{\mathrm{str}}}{\partial \boldsymbol{F}_{\mathrm{p}}}\right) = \boldsymbol{C}\left(2\Phi_{1\mathrm{s}\nu}\frac{\partial \tilde{W}_{\mathrm{str}}}{\partial \boldsymbol{C}}\right)$$
$$= \left\langle\!\!\left\langle f\mathrm{Dev}\left(\boldsymbol{C}\boldsymbol{F}_{\mathrm{p}}^{-1}\mathfrak{a}\boldsymbol{F}_{\mathrm{p}}^{-\mathrm{T}}\right)\right\rangle\!\!\right\rangle, \tag{23b}$$
$$\boldsymbol{\Sigma}_{\mathrm{Grad}} = -\boldsymbol{F}_{\mathrm{p}}^{\mathrm{T}}\left(\Phi_{1\mathrm{s}\nu}\frac{\partial \tilde{W}_{\mathrm{Grad}}}{\partial \boldsymbol{F}_{\mathrm{p}}}\right) = \mathrm{Grad}\,\mathfrak{q}\otimes\left(\Phi_{1\mathrm{s}\nu}\frac{\partial \tilde{W}_{\mathrm{Grad}}}{\partial\,\mathrm{Grad}\,\mathfrak{q}}\right), \tag{23c}$$

where the factor f is defined by

$$f = 2\Phi_{1\mathrm{s}\nu}\mathscr{A}_0\mathscr{P}(\mathfrak{q})I_{3\mathrm{e}}^{-1/3}k_2[\bar{I}_{4\mathrm{e}}-1]\exp\left(k_2[\bar{I}_{4\mathrm{e}}-1]^2\right)\mathcal{H}(I_{4\mathrm{e}}-1). \tag{24}$$

Hence, we obtain the residual dissipation inequality

$$\mathfrak{D}_{\mathrm{res}} = -\phi_{\mathrm{f}}^{-1}\boldsymbol{\pi}_{\mathrm{fd}}.\boldsymbol{F}\boldsymbol{\mathcal{Q}} + \left\{y^{(0)} - \frac{\partial \tilde{W}_{\nu}}{\partial \mathfrak{q}}\right\}\dot{\mathfrak{q}} + \left\{\boldsymbol{y}^{(1)} - \frac{\partial \tilde{W}_{\nu}}{\partial \mathrm{Grad}\mathfrak{q}}\right\}\mathrm{Grad}\dot{\mathfrak{q}}$$
$$+ \left\{\boldsymbol{F}_{\mathrm{p}}^{-\mathrm{T}}\left(\boldsymbol{F}_{\mathrm{p}}^{\mathrm{T}}\boldsymbol{Y}_{\nu}^{\mathrm{int}} + \boldsymbol{\Sigma}_{\mathrm{std}} + \boldsymbol{\Sigma}_{\mathrm{str}} + \boldsymbol{\Sigma}_{\mathrm{Grad}}\right)\boldsymbol{F}_{\mathrm{p}}^{\mathrm{T}}\right\} : \boldsymbol{L}_{\mathrm{p}} \geq 0, \tag{25}$$

where $\boldsymbol{\pi}_{\mathrm{fd}}$ is the force density describing the exchange of linear momentum between the solid and the fluid, and $\boldsymbol{\mathcal{Q}} = J\boldsymbol{F}^{-1}\boldsymbol{q}$ is referred to as *material filtration velocity*, i.e., the backward Piola-transformation of the filtration velocity $\boldsymbol{q} = \phi_{\mathrm{f}}[\boldsymbol{v}_{\mathrm{f}} - \boldsymbol{v}_{\mathrm{s}}]$.

With reference to (23a)–(23c), $\boldsymbol{\Sigma}_{\mathrm{std}}$ can be found in several theories on remodelling available in the literature (see e.g. [21, 22]); $\boldsymbol{\Sigma}_{\mathrm{str}}$ represents a *structural* generalised force that descends from the coupling between the deformation and the evolution of the fibres accounted for by W_{str}; $\boldsymbol{\Sigma}_{\mathrm{Grad}}$ stems from the coupling of the plastic-like distortions with the evolution of the fibres, and is a direct consequence of the introduction of the free energy density W_{Grad}.

Tensor $\boldsymbol{\Sigma}_{\mathrm{Grad}}$ can be interpreted as a generalisation of the Korteweg stress tensor. Coherently with W_{Grad}, it represents a generalised configurational force that is power-conjugate to $\boldsymbol{L}_{\mathrm{p}} = \dot{\boldsymbol{F}}_{\mathrm{p}}\boldsymbol{F}_{\mathrm{p}}^{-1}$, and that results from the coupling between $\boldsymbol{F}_{\mathrm{p}}$ and $\mathfrak{q}$. We also remark that, since in our model W_{Grad} is independent of $\boldsymbol{C}$, the differentiation of W_{Grad} with respect to $\boldsymbol{C}$ is null, thereby implying that W_{Grad} does not contribute to the second Piola-Kirchhoff stress tensor of the solid. Therefore, $\boldsymbol{\Sigma}_{\mathrm{Grad}}$ cannot possess the same properties as the Mandel stress tensors $\boldsymbol{\Sigma}_{\mathrm{std}}$ and $\boldsymbol{\Sigma}_{\mathrm{str}}$ defined in (23a) and (23b), respectively. For instance, it cannot be written in terms of the product of

$\boldsymbol{C}$ with $(2\Phi_{1s\nu}\partial\tilde{W}_{\mathrm{Grad}}/\partial\boldsymbol{C})$, and it does not fulfil the symmetry conditions $\boldsymbol{\Sigma}_{\mathrm{std}}\boldsymbol{C} = (\boldsymbol{\Sigma}_{\mathrm{std}}\boldsymbol{C})^{\mathrm{T}}$ and $\boldsymbol{\Sigma}_{\mathrm{str}}\boldsymbol{C} = (\boldsymbol{\Sigma}_{\mathrm{str}}\boldsymbol{C})^{\mathrm{T}}$. These stem from the coupling among $\boldsymbol{F}$, $\boldsymbol{F}_{\mathrm{p}}$, and $\mathfrak{q}$, a coupling that is accounted for by $\tilde{W}_{\mathrm{std}}$ and $\tilde{W}_{\mathrm{str}}$, but not by $\tilde{W}_{\mathrm{Grad}}$. We notice that $\boldsymbol{\Sigma}_{\mathrm{Grad}}$ satisfies the symmetry conditions $\boldsymbol{B}_{\mathrm{p}}\boldsymbol{\Sigma}_{\mathrm{Grad}} = (\boldsymbol{B}_{\mathrm{p}}\boldsymbol{\Sigma}_{\mathrm{Grad}})^{\mathrm{T}}$ [51].

In (25), we perform the identification

$$\boldsymbol{y}^{(1)} = \frac{\partial\tilde{W}_{\nu}}{\partial\mathrm{Grad}\mathfrak{q}} = \Phi_{1s\nu}D_0\boldsymbol{B}_{\mathrm{p}}\mathrm{Grad}\mathfrak{q}, \tag{26}$$

which amounts to require that $\boldsymbol{y}^{(1)}$ has no dissipative contribution, and, by recalling the definition of $\mathscr{R}_{\nu}^{\mathrm{int}}$ given in (5b), we introduce the dissipative parts of the internal generalised forces $\mathscr{R}_{\nu}^{\mathrm{int}}$ and $\boldsymbol{Y}_{\nu}^{\mathrm{int}}$:

$$\mathscr{R}_{\nu,\mathrm{d}}^{\mathrm{int}} := y^{(0)} - \frac{\partial\tilde{W}_{\nu}}{\partial\mathfrak{q}} = \mathscr{R}_{\nu}^{\mathrm{int}} - \mathscr{E}(\mathfrak{q}, \mathrm{Grad}\,\mathfrak{q}), \tag{27a}$$

$$\boldsymbol{F}_{\mathrm{p}}^{\mathrm{T}}\boldsymbol{Y}_{\nu,\mathrm{d}}^{\mathrm{int}} := \mathrm{dev}(\boldsymbol{F}_{\mathrm{p}}^{\mathrm{T}}\boldsymbol{Y}_{\nu}^{\mathrm{int}}) + \mathrm{dev}(\boldsymbol{\Sigma}_{\mathrm{std}} + \boldsymbol{\Sigma}_{\mathrm{str}} + \boldsymbol{\Sigma}_{\mathrm{Grad}}), \tag{27b}$$

where $\mathscr{E}(\mathfrak{q}, \mathrm{Grad}\,\mathfrak{q})$ is the scalar generalised force given by

$$\mathscr{E}(\mathfrak{q}, \mathrm{Grad}\,\mathfrak{q}) := \frac{\partial\tilde{W}_{\nu}}{\partial\mathfrak{q}} - \mathrm{Div}\left(\frac{\partial\tilde{W}_{\nu}}{\partial\,\mathrm{Grad}\,\mathfrak{q}}\right). \tag{28}$$

Hence, $\mathfrak{D}_{\mathrm{res}}$ becomes

$$\mathfrak{D}_{\mathrm{res}} = -\,\phi_{\mathrm{f}}^{-1}\boldsymbol{\pi}_{\mathrm{fd}}.\boldsymbol{F}\boldsymbol{\mathcal{Q}} + \mathscr{R}_{\nu,\mathrm{d}}^{\mathrm{int}}\dot{\mathfrak{q}} + \boldsymbol{F}_{\mathrm{p}}^{-\mathrm{T}}\left(\boldsymbol{F}_{\mathrm{p}}^{\mathrm{T}}\boldsymbol{Y}_{\nu,\mathrm{d}}^{\mathrm{int}}\right)\boldsymbol{F}_{\mathrm{p}}^{\mathrm{T}} : \boldsymbol{L}_{\mathrm{p}} \geq 0. \tag{29}$$

By recalling the force balances (2), reformulated for the case of isochoric plastic-like distortions, and (6), which allow to substitute $\mathscr{R}_{\nu}^{\mathrm{int}}$ with $\mathscr{R}_{\nu}^{\mathrm{ext}}$ in (27a) and $\boldsymbol{Y}_{\nu}^{\mathrm{int}}$ with $\boldsymbol{Y}_{\nu}^{\mathrm{ext}}$ in (27b), we obtain [24, 33, 50]

$$\mathscr{R}_{\nu,\mathrm{d}}^{\mathrm{int}} = \mathscr{R}_{\nu}^{\mathrm{ext}} - \mathscr{E}(\mathfrak{q}, \mathrm{Grad}\,\mathfrak{q}), \tag{30a}$$

$$\boldsymbol{F}_{\mathrm{p}}^{\mathrm{T}}\boldsymbol{Y}_{\nu,\mathrm{d}}^{\mathrm{int}} = \mathrm{dev}(\boldsymbol{F}_{\mathrm{p}}^{\mathrm{T}}\boldsymbol{Y}_{\nu}^{\mathrm{ext}}) + \mathrm{dev}(\boldsymbol{\Sigma}_{\mathrm{std}} + \boldsymbol{\Sigma}_{\mathrm{str}} + \boldsymbol{\Sigma}_{\mathrm{Grad}}). \tag{30b}$$

If $\mathscr{R}_{\nu,\mathrm{d}}^{\mathrm{int}}$ and $\boldsymbol{Y}_{\nu,\mathrm{d}}^{\mathrm{int}}$ can be related constitutively to $\dot{\mathfrak{q}}$ and $\boldsymbol{L}_{\mathrm{p}}$, respectively, (30a) and (30b) become evolution laws for $\mathfrak{q}$ and $\boldsymbol{F}_{\mathrm{p}}$. For this purpose, we study the dissipation inequality, and we require here each summand of (29) to be

non-negative independently on the other ones [29], i.e.,

$$\mathfrak{D}_{\text{flow}} = -\phi_{\text{f}}^{-1}\boldsymbol{\pi}_{\text{fd}}.\boldsymbol{F}\boldsymbol{\mathcal{Q}} \geq 0, \tag{31a}$$

$$\mathfrak{D}_{\mathfrak{q}} = \mathscr{R}^{\text{int}}_{\nu,\text{d}}\dot{\mathfrak{q}} \geq 0, \tag{31b}$$

$$\mathfrak{D}_{\text{p}} = \boldsymbol{F}_{\text{p}}^{-\text{T}}\left(\boldsymbol{F}_{\text{p}}^{\text{T}}\boldsymbol{Y}^{\text{int}}_{\nu,\text{d}}\right)\boldsymbol{F}_{\text{p}}^{\text{T}} : \boldsymbol{L}_{\text{p}} \geq 0. \tag{31c}$$

First, we consider the inequality $\mathfrak{D}_{\text{flow}} \geq 0$, and, by hypothesising a linear relationship between $\boldsymbol{\pi}_{\text{fd}}$ and $\boldsymbol{\mathcal{Q}}$ [52, 53], we obtain Darcy's law, i.e.,

$$\boldsymbol{\mathcal{Q}} = -\boldsymbol{K}\,\text{Grad}\,p. \tag{32}$$

Then, to satisfy $\mathfrak{D}_{\mathfrak{q}} \geq 0$, we assume $\mathscr{R}^{\text{int}}_{\nu,\text{d}} = \Gamma\dot{\mathfrak{q}}$, with Γ being a stricitly positive quantity (in general, it sufficies that Γ be non-negative).

Finally, we turn to $\mathfrak{D}_{\text{p}}$, and we assume that the plastic-like distortions evolve according to a modified rate-independent formulation of plasticity, compatible with an associative normality rule [54]. Moreover, we hypothesise that $\boldsymbol{Y}^{\text{ext}}_{\nu}$ is identically null [36] and, by performing the change of variable $\boldsymbol{H} = \boldsymbol{F}_{\text{p}}^{-1}$ and setting $\boldsymbol{\Lambda} = \dot{\boldsymbol{H}}\boldsymbol{H}^{-1}$, we obtain

$$\boldsymbol{H}^{-\text{T}}\boldsymbol{Y}^{\text{int}}_{\nu,\text{d}} = \text{dev}(\boldsymbol{\Sigma}_{\text{std}} + \boldsymbol{\Sigma}_{\text{str}} + \boldsymbol{\Sigma}_{\text{Grad}}) \equiv \text{dev}\boldsymbol{\Sigma}_{\text{eff}}, \tag{33a}$$

$$\mathfrak{D}_{\text{p}} = -\boldsymbol{\Sigma}_{\text{eff}} : \boldsymbol{\Lambda} = -(\text{dev}\boldsymbol{\Sigma}_{\text{eff}}) : \boldsymbol{\Lambda} \geq 0, \tag{33b}$$

where $\boldsymbol{\Sigma}_{\text{eff}}$ is referred to as the *effective* Mandel-like stress tensor and is the sum of $\boldsymbol{\Sigma}_{\text{std}}$, $\boldsymbol{\Sigma}_{\text{str}}$, and $\boldsymbol{\Sigma}_{\text{Grad}}$. We remark that, because of the constraint $\det\boldsymbol{H} = 1$, $\boldsymbol{\Lambda}$ is deviatoric and, consequently, it selects only the deviatoric part of $\boldsymbol{\Sigma}_{\text{eff}}$ in $\mathfrak{D}_{\text{p}}$.

Next, we use $\boldsymbol{\Sigma}_{\text{eff}}$ to define the *effective* Cauchy-like stress tensor

$$\boldsymbol{\sigma}_{\text{eff}} := J^{-1}\boldsymbol{g}^{-1}\boldsymbol{F}^{-\text{T}}\boldsymbol{\Sigma}_{\text{eff}}\boldsymbol{F}^{\text{T}}. \tag{34}$$

We remark that, because of the presence of $\boldsymbol{\Sigma}_{\text{Grad}}$, $\boldsymbol{\Sigma}_{\text{eff}}$ is *not* a true Mandel stress tensor and, analogously, $\boldsymbol{\sigma}_{\text{eff}}$ is *not* a true Cauchy stress tensor. Rather, $\boldsymbol{\sigma}_{\text{eff}}$ only represents the spatial counterpart of $\boldsymbol{\Sigma}_{\text{eff}}$, constructed as shown in (34), but it does not necessarily satisfy the properties that a true Cauchy stress tensor should fulfil. For example, it is not symmetric. Still, we employ $\boldsymbol{\sigma}_{\text{eff}}$ to formulate a yield criterion of the von Mises type. To this end, we

introduce the yield function

$$\mathscr{Y} = \|\mathrm{dev}\boldsymbol{\sigma}_{\mathrm{eff}}\|_{\boldsymbol{g}} - \sqrt{(2/3)}\,\sigma_y, \tag{35}$$

where σ_y is a strictly positive yield stress, and, to comply with the condition $J_{\mathrm{p}} = 1$, only the deviatoric part of $\boldsymbol{\sigma}_{\mathrm{eff}}$ is considered. We remark that the norm $\|\mathrm{dev}\boldsymbol{\sigma}_{\mathrm{eff}}\|_{\boldsymbol{g}}$ is computed with respect to the spatial metric $\boldsymbol{g}$, i.e.,

$$\|\mathrm{dev}\boldsymbol{\sigma}_{\mathrm{eff}}\|_{\boldsymbol{g}} = \sqrt{\boldsymbol{g} : (\mathrm{dev}\boldsymbol{\sigma}_{\mathrm{eff}})\boldsymbol{g}(\mathrm{dev}\boldsymbol{\sigma}_{\mathrm{eff}})^{\mathrm{T}}}. \tag{36}$$

By expressing the norm $\|\mathrm{dev}\boldsymbol{\sigma}_{\mathrm{eff}}\|_{\boldsymbol{g}}$ in terms of $\boldsymbol{\Sigma}_{\mathrm{eff}}$, i.e.,

$$\|\mathrm{dev}\boldsymbol{\sigma}_{\mathrm{eff}}\|_{\boldsymbol{g}} = J^{-1}\|\mathrm{dev}\boldsymbol{\Sigma}_{\mathrm{eff}}\|_{\boldsymbol{C}}, \tag{37a}$$

$$\|\mathrm{dev}\boldsymbol{\Sigma}_{\mathrm{eff}}\|_{\boldsymbol{C}} := \sqrt{\boldsymbol{C}^{-1} : (\mathrm{dev}\boldsymbol{\Sigma}_{\mathrm{eff}})\boldsymbol{C}(\mathrm{dev}\boldsymbol{\Sigma}_{\mathrm{eff}})^{\mathrm{T}}}, \tag{37b}$$

we rephrase $\mathscr{Y}$ in terms of $\boldsymbol{\Sigma}_{\mathrm{eff}}$ and $\boldsymbol{C}$, thereby obtaining

$$\mathscr{Y} = \hat{\mathscr{Y}}(\boldsymbol{C}, \boldsymbol{\Sigma}_{\mathrm{eff}}) = J^{-1}\|\mathrm{dev}\boldsymbol{\Sigma}_{\mathrm{eff}}\|_{\boldsymbol{C}} - \sqrt{(2/3)}\,\sigma_y. \tag{38}$$

We use (38) to maximise $\mathfrak{D}_{\mathrm{p}}$ over all the possible stresses [55]. For this purpose, we adopt the Karush-Kuhn-Tucker technique [55], along with the modified dissipation

$$\tilde{\mathfrak{D}}_{\mathrm{p}}(\boldsymbol{C}, \boldsymbol{\Sigma}_{\mathrm{eff}}, \lambda) = -\mathrm{dev}\boldsymbol{\Sigma}_{\mathrm{eff}} : \boldsymbol{\Lambda} - \lambda\hat{\mathscr{Y}}(\boldsymbol{C}, \boldsymbol{\Sigma}_{\mathrm{eff}}) \geq 0, \tag{39}$$

where λ is a Karush-Kuhn-Tucker (KKT) multiplier, to be determined. The search for maximisers of $\tilde{\mathfrak{D}}_{\mathrm{p}}(\boldsymbol{C}, \boldsymbol{\Sigma}_{\mathrm{eff}}, \lambda)$ is accomplished by differentiating $\tilde{\mathfrak{D}}_{\mathrm{p}}$ with respect to $\boldsymbol{\Sigma}_{\mathrm{eff}}$ and λ, and leads to the Karush-Kuhn-Tucker optimality conditions [55]. Since in this work the yield stress, σ_y, is assumed to be a given model parameter, such optimality conditions read

$$\frac{\partial\tilde{\mathfrak{D}}_{\mathrm{p}}}{\partial\boldsymbol{\Sigma}_{\mathrm{eff}}}(\boldsymbol{C}, \boldsymbol{\Sigma}_{\mathrm{eff}}, \lambda) = -\boldsymbol{\Lambda} - \lambda\frac{\partial\hat{\mathscr{Y}}}{\partial\boldsymbol{\Sigma}_{\mathrm{eff}}}(\boldsymbol{C}, \boldsymbol{\Sigma}_{\mathrm{eff}}) = \boldsymbol{0}, \tag{40a}$$

$$\lambda \geq 0, \qquad \hat{\mathscr{Y}}(\boldsymbol{C}, \boldsymbol{\Sigma}_{\mathrm{eff}}) \leq 0, \qquad \lambda\hat{\mathscr{Y}}(\boldsymbol{C}, \boldsymbol{\Sigma}_{\mathrm{eff}}) = 0. \tag{40b}$$

5.1. Reorientation of the fibres

By substituting $\mathscr{R}^{\text{int}}_{\nu,\text{d}} = \Gamma\dot{\mathfrak{q}}$ into (30a), and writing $\mathscr{E}(\mathfrak{q}, \text{Grad}\,\mathfrak{q})$ explicitly, Eq. (30a) takes on the form

$$\Gamma\dot{\mathfrak{q}} = \text{Div}\,[\Phi_{1\text{s}\nu} D_0 \boldsymbol{B}_\text{p} \text{Grad}\,\mathfrak{q}] - \Phi_{1\text{s}\nu}\frac{\partial(\hat{W}_{1\text{a}} + \hat{W}_{\text{str}})}{\partial\mathfrak{q}} + \mathscr{R}^{\text{ext}}_{\nu}. \tag{41}$$

The first term on the right-hand-side of (41) contributes to the evolution of the fibre mean angle by resolving the spatial variability of $\mathfrak{q}$. The coefficient $\Phi_{1\text{s}\nu} D_0$ multiplies the inverse (plastic) metric tensor $\boldsymbol{B}_\text{p}$, thereby leading to the tensorial coefficient $\Phi_{1\text{s}\nu} D_0 \boldsymbol{B}_\text{p}$. We notice that, in spite of some formal similarities with a diffusion-reaction equation, (41) describes no diffusion, since it is not a mass balance, but the evolution of an order parameter [56].

To solve (41), we need to provide $\mathscr{R}^{\text{ext}}_{\nu}$. In two previous papers on this subject [24, 40], one of us reviewed some results presented by other authors, e.g. [32, 33], who defined the external remodelling force $\mathscr{R}^{\text{ext}}_{\nu}$ by introducing the concept of *target angle*, $\mathfrak{q}_T$. The target angle is an angle that defines the direction of space, which we may call *target direction*, along which the fibres "would like to be aligned". By definition, the fibres tend to orient themselves along the target direction and it has been observed that, in a tissue subjected to mechanical stress and deformation, the target angle depends on stress [32, 33] or deformation [12, 31].

Although the issue of the target angle was discussed in [24, 40], the focus in those papers was on the particular situations in which no external force $\mathscr{R}^{\text{ext}}_{\nu}$ was active, i.e., when the condition $\mathscr{R}^{\text{ext}}_{\nu} = 0$ applies in (41). In these cases, indeed, a "target angle" may be identified with a stationary solution of (41), i.e., a function $\mathfrak{q}_\infty$ satisfying

$$\text{Div}\,[\Phi_{1\text{s}\nu} D_0 \boldsymbol{B}_\text{p} \text{Grad}\,\mathfrak{q}] - \Phi_{1\text{s}\nu}\frac{\partial(\hat{W}_{1\text{a}} + \hat{W}_{\text{str}})}{\partial\mathfrak{q}} = 0, \tag{42}$$

together with time-independent boundary conditions. Since $\partial\hat{W}_{\text{str}}/\partial\mathfrak{q}$ does not vanish when $\boldsymbol{B}_\text{p} = \boldsymbol{G}^{-1}$ and the tissue is undeformed, (42) admits solutions of sigmoidal shape that interpolate between the zeroes of the double-well potential $\mathscr{P}(\mathfrak{q})$, i.e., $\mathfrak{q}_0 = 0$ and $\mathfrak{q}_1 = \pi/2$. Always in the absence of deformation, such profiles can also be obtained as the stationary solutions of (41), when the initial distribution of $\mathfrak{q}$ is a random function of material points [24].

In the case of vanishing D_0, the energy density W_{Grad} is null, and we end up with a description of remodelling determined by ordinary differential equations. In such situations, and for $\mathscr{R}_\nu^{\mathrm{ext}} = 0$, the search for stationary solutions amounts to seek for the zeros of the equation

$$-\Phi_{1\mathrm{s}\nu}\frac{\partial(\hat{W}_{1\mathrm{a}} + \hat{W}_{\mathrm{str}})}{\partial \mathfrak{q}} = 0. \tag{43}$$

In general, however, (43) may admit either no solutions or multiple solutions, i.e., different target angles. Whereas the existence of multiple stationary solutions to (43) can be a normal fact, because the Cauchy problem

$$\Gamma\dot{\mathfrak{q}} = -\Phi_{1\mathrm{s}\nu}\frac{\partial(\hat{W}_{1\mathrm{a}} + \hat{W}_{\mathrm{str}})}{\partial \mathfrak{q}}, \tag{44a}$$

$$\mathfrak{q}(X, 0) = \mathfrak{q}_{\mathrm{in}}(X), \tag{44b}$$

if well-posed, selects a unique solution, the case of no stationary solution may be unphysical. Similar circumstances may occur when the right-hand-side of (44a) features only $\partial\hat{W}_{1\mathrm{a}}/\partial\mathfrak{q}$.

By introducing a non-vanishing $\mathscr{R}_\nu^{\mathrm{ext}}$, relating it to the concept of an *a priori* defined target angle, $\mathfrak{q}_T$, and assuming the existence of a stationary limit $\mathfrak{q}_T^\infty$, the unphysical case of no stationary solutions is eliminated at source. Indeed, it suffices to notice that a stationary angle is attained when the external force $\mathscr{R}_\nu^{\mathrm{ext}}$ balances the internal ones under the condition $\dot{\mathfrak{q}} = 0$. This implies that the following equality has to be verified [33]

$$\mathscr{R}_\nu^{\mathrm{ext}} = \Phi_{1\mathrm{s}\nu}\left.\frac{\partial(\hat{W}_{1\mathrm{a}} + \hat{W}_{\mathrm{str}})}{\partial \mathfrak{q}}\right|_{\mathfrak{q}=\mathfrak{q}_T^\infty}. \tag{45}$$

This result can also be generalised to the case in which the target angle is not stationary, so that Eq. (44a) is rewritten as

$$\Gamma\dot{\mathfrak{q}} = -\Phi_{1\mathrm{s}\nu}\frac{\partial(\hat{W}_{1\mathrm{a}} + \hat{W}_{\mathrm{str}})}{\partial \mathfrak{q}} + \Phi_{1\mathrm{s}\nu}\left.\frac{\partial(\hat{W}_{1\mathrm{a}} + \hat{W}_{\mathrm{str}})}{\partial \mathfrak{q}}\right|_{\mathfrak{q}=\mathfrak{q}_T}, \tag{46}$$

where the term on the right-hand-side iscomputed for a non-stationary target angle $\mathfrak{q}_T$, driven by stress or deformation.

Even more generally, when the remodelling equation is given by (41), the external force $\mathscr{R}_\nu^{\rm ext}$ may be defined as

$$\begin{aligned}\mathscr{R}_\nu^{\rm ext} &= \mathscr{E}(q_{\rm T}, {\rm Grad}\,\mathfrak{q}_T)\\ &= -{\rm Div}\,[\Phi_{1{\rm s}\nu} D_0 \boldsymbol{B}_{\rm p} {\rm Grad}\mathfrak{q}_T] + \Phi_{1{\rm s}\nu}\left.\frac{\partial(\hat{W}_{1{\rm a}} + \hat{W}_{\rm str})}{\partial \mathfrak{q}}\right|_{\mathfrak{q}=\mathfrak{q}_T},\end{aligned} \tag{47}$$

thereby obtaining the following generalisation of [24, 33, 40]:

$$\begin{aligned}\Gamma\dot{\mathfrak{q}} =& {\rm Div}\,[\Phi_{1{\rm s}\nu} D_0 \boldsymbol{B}_{\rm p} {\rm Grad}\,\mathfrak{q}] - \Phi_{1{\rm s}\nu}\frac{\partial(\hat{W}_{1{\rm a}} + \hat{W}_{\rm str})}{\partial \mathfrak{q}}\\ &- {\rm Div}\,[\Phi_{1{\rm s}\nu} D_0 \boldsymbol{B}_{\rm p} {\rm Grad}\,\mathfrak{q}_T] + \Phi_{1{\rm s}\nu}\left.\frac{\partial(\hat{W}_{1{\rm a}} + \hat{W}_{\rm str})}{\partial \mathfrak{q}}\right|_{\mathfrak{q}=\mathfrak{q}_T}.\end{aligned} \tag{48}$$

5.2. Evolution of the plastic-like distortions

The explicit computation of the derivative of $\hat{\mathscr{Y}}$ with respect to $\boldsymbol{\Sigma}_{\rm eff}$, see (38), permits to rewrite (40a) as

$$\boldsymbol{\Lambda} = -J^{-1}\lambda\,\frac{\boldsymbol{C}^{-1}({\rm dev}\boldsymbol{\Sigma}_{\rm eff})\boldsymbol{C}}{\|{\rm dev}\boldsymbol{\Sigma}_{\rm eff}\|_{\boldsymbol{C}}}, \tag{49}$$

which implies $\|\boldsymbol{\Lambda}\|_{\boldsymbol{C}} \equiv \sqrt{\boldsymbol{C} : \boldsymbol{\Lambda}\boldsymbol{C}^{-1}\boldsymbol{\Lambda}^{\rm T}} = J^{-1}\lambda \geq 0$. Moreover, since $\boldsymbol{\Lambda}$ is given by $\boldsymbol{\Lambda} = \dot{\boldsymbol{H}}\boldsymbol{H}^{-1}$, (49) can be recast in the form of an evolution equation for $\boldsymbol{H}$ or, equivalently, for $\boldsymbol{F}_{\rm p} = \boldsymbol{H}^{-1}$, i.e.,

$$\dot{\boldsymbol{H}} = \left\{-J^{-1}\lambda\,\frac{\boldsymbol{C}^{-1}({\rm dev}\boldsymbol{\Sigma}_{\rm eff})\boldsymbol{C}}{\|{\rm dev}\boldsymbol{\Sigma}_{\rm eff}\|_{\boldsymbol{C}}}\right\}\boldsymbol{H}. \tag{50}$$

Within the classical framework of finite Elastoplasticity, the KKT-multiplier λ is determined by enforcing a condition known as "consistency condition" [55], which has to be solved together with the flow rule —represented here by (50)— and the other model equations. Very often, the consistency condition is solved algorithmically (see e.g. [55]). In this work, however, we propose a rather different approach, which is motivated by the need of keeping our calculations at a minimum level of complexity (see Sect. 5.3 for some technical details on this issue). In fact, we prescribe λ from the outset, and, for our

purposes, we define it as

$$\begin{aligned}\lambda &= J\zeta_0\phi_{\mathrm{s}}\left[\|\mathrm{dev}\boldsymbol{\sigma}_{\mathrm{eff}}\|_{\boldsymbol{g}} - \sqrt{(2/3)}\,\sigma_y\right]_+ \\ &= \zeta_0\Phi_{\mathrm{s}\nu}\left[J^{-1}\|\mathrm{dev}\boldsymbol{\Sigma}_{\mathrm{eff}}\|_{\boldsymbol{C}} - \sqrt{(2/3)}\,\sigma_y\right]_+ ,\end{aligned} \tag{51}$$

where $\zeta_0 > 0$ is a constant model parameter, and $[A]_+ = A$, for $A > 0$, and $[A]_+ = 0$, otherwise. We notice that the equality $\Phi_{\mathrm{s}\nu} = J\phi_{\mathrm{s}}$ is verified, because it holds that $J = J_{\mathrm{e}}$, since the condition $J_{\mathrm{p}} = 1$ applies. Finally, by substituting (51) into (50), we obtain

$$\dot{\boldsymbol{H}} = -\frac{\zeta_0\Phi_{\mathrm{s}\nu}\left[J^{-1}\|\mathrm{dev}\boldsymbol{\Sigma}_{\mathrm{eff}}\|_{\boldsymbol{C}} - \sqrt{(2/3)}\,\sigma_y\right]_+}{J}\,\frac{\boldsymbol{C}^{-1}(\mathrm{dev}\boldsymbol{\Sigma}_{\mathrm{eff}})\boldsymbol{C}}{\|\mathrm{dev}\boldsymbol{\Sigma}_{\mathrm{eff}}\|_{\boldsymbol{C}}}\boldsymbol{H}, \tag{52}$$

i.e., the ordinary differential equation describing the evolution of $\boldsymbol{H}$.

Equation (52) looks like an evolution law of the Norton-Hoff type [57] and, with some modifications, might be rated among those. However, compared with that in [57], our (52) features three differences: (i) the full tensor $\mathrm{dev}\boldsymbol{\Sigma}_{\mathrm{eff}}$ is considered in lieu of its symmetric part only (see [57] for some remarks on this issue); (ii) the "transformed" generalised stress $\boldsymbol{C}^{-1}\mathrm{dev}\boldsymbol{\Sigma}_{\mathrm{eff}}\boldsymbol{C}$, rather than $\mathrm{dev}\boldsymbol{\Sigma}_{\mathrm{eff}}$, is regarded as the driving force for $\boldsymbol{H}$; (iii) our $\boldsymbol{\Sigma}_{\mathrm{eff}}$ contains $\boldsymbol{\Sigma}_{\mathrm{Grad}}$, which is a fundamental character of our framework.

We notice that the coefficient λ in (51) has the form of the activation factor featuring in the flow rule of a Perzyna-like model of viscoplasticity [37]. Dimensional analysis shows that the parameter ζ_0 can be expressed as $\zeta_0 = (\tau_{\mathrm{c}}\sigma_{\mathrm{c}})^{-1}$, where τ_{c} is the characteristic relaxation time of $\boldsymbol{H}$, and σ_{c} is a reference value of stress. The time scale τ_{c} is available in the literature, and we choose $\tau_{\mathrm{c}} = 22\,\mathrm{s}$, as suggested in [28], where the inelastic behaviour of cellular aggregates is studied by means of a Perzyna-like flow rule. However, there seems to be some freedom in the choice of the reference stress σ_{c}. In principle, indeed, σ_{c} could be taken equal to σ_y, if one wants to normalise λ with the yield stress, or it could be defined by combining the material parameters involved in the definition of $\boldsymbol{\sigma}_{\mathrm{eff}}$. In the latter case, one should use parameters, such as D_0 and $\mathscr{A}_0$, that, being other than the standard elastic coefficients, are not available in the literature, at least to the best of our knowledge. Thus, we refer here to a value of σ_{c} that has already been used in [28], within a framework similar to ours. To this end, by comparing (51)

with the flow rule in [28], we identify $\sigma_{\rm c}$ with $\sigma_{\rm c} = 2\mu_0\langle\Phi_{{\rm s}\nu}\rangle$, where μ_0 is the shear modulus of the matrix, and $\langle\Phi_{{\rm s}\nu}\rangle$ is the mean value of the solid phase volumetric ratio. Hence, upon computing $\mu_0 = 2(\alpha_1+\alpha_2)\alpha_0 \approx 0.222\,\mathrm{MPa}$ [41] and $\langle\Phi_{{\rm s}\nu}\rangle = \int_0^1 \Phi_{{\rm s}\nu}(\xi)\mathrm{d}\xi = 0.2$ (see Table 1), we find $\sigma_{\rm c} \approx 0.09\,\mathrm{MPa}$ and $\zeta_0 \approx 0.50\,\mathrm{MPa}^{-1}\mathrm{s}^{-1}$ (cf. Table 1). Such $\sigma_{\rm c}$ is obtained by considering only the isotropic part of the standard energy of our model, whereas considering also the other terms of the energy would lead to higher values of $\sigma_{\rm c}$ and, then, to smaller values of ζ_0. On the other hand, smaller values of $\sigma_{\rm c}$ are conceivable, but they could result into too high values of ζ_0 for the problem at hand, thereby leading to unphysical time scales for the evolution of $\boldsymbol{H}$.

5.3. Summary of the model equations and technical details

After enforcing the left polar decomposition of $\boldsymbol{H}$, i.e., $\boldsymbol{H} = \boldsymbol{V}.\boldsymbol{R}$ [35], we study only the case in which $\boldsymbol{R}$ reduces to a shifter [35], so that the unknown determining the plastic-like distortions becomes the symmetric, second-order tensor $\boldsymbol{V}$. Even though this choice has the disadvantage of restricting the investigation to the case of no plastic-like rotations, it allows to work with $\boldsymbol{V}$, which, being symmetric, is computationally cheaper. In summary, thus, our mathematical model consists of the following set of four, highly non-linear, coupled equations,

$$\dot{J} - \mathrm{Div}\,(\boldsymbol{K}\mathrm{Grad}\,p) = 0, \tag{53a}$$

$$\mathrm{Div}\left(-J\,p\,\boldsymbol{g}^{-1}\boldsymbol{F}^{-\mathrm{T}} + \boldsymbol{P}_{\rm sc}\right) = \boldsymbol{0}, \tag{53b}$$

$$\begin{aligned}\Gamma\dot{\mathfrak{q}} = {}& \mathrm{Div}\,[\Phi_{1{\rm s}\nu}D_0\boldsymbol{B}_{\rm p}\mathrm{Grad}\,\mathfrak{q}] - \Phi_{1{\rm s}\nu}\frac{\partial(\hat{W}_{1\rm a}+\hat{W}_{\rm str})}{\partial\mathfrak{q}} \\ & - \mathrm{Div}\,[\Phi_{1{\rm s}\nu}D_0\boldsymbol{B}_{\rm p}\mathrm{Grad}\,\mathfrak{q}_T] + \Phi_{1{\rm s}\nu}\left.\frac{\partial(\hat{W}_{1\rm a}+\hat{W}_{\rm str})}{\partial\mathfrak{q}}\right|_{\mathfrak{q}=\mathfrak{q}_T},\end{aligned} \tag{53c}$$

$$\dot{\boldsymbol{V}} = -\mathrm{sym}\left[\left(\frac{\lambda}{J}\frac{\boldsymbol{C}^{-1}(\mathrm{dev}\boldsymbol{\Sigma}_{\rm eff})\boldsymbol{C}}{\|\mathrm{dev}\boldsymbol{\Sigma}_{\rm eff}\|_{\boldsymbol{C}}}\right)\boldsymbol{V}\right], \tag{53d}$$

in the unknowns p, χ, $\mathfrak{q}$, and $\boldsymbol{V}$, respectively. Note that we take the symmetric part of the right-hand-side of (53d) in order to ensure that $\dot{\boldsymbol{V}}$, and its time discrete form, be symmetric. Moreover, the material permeability is given by [41, 6, 8, 9]

$$\boldsymbol{K} = k_0\frac{(J-\Phi_{1{\rm s}\nu})^2}{J}\boldsymbol{C}^{-1} + k_0\frac{(J-\Phi_{1{\rm s}\nu})\Phi_{1{\rm s}\nu}}{J}\boldsymbol{H}\left\langle\!\!\left\langle\frac{\mathfrak{a}}{I_{4\rm e}}\right\rangle\!\!\right\rangle\boldsymbol{H}^{\mathrm{T}}, \tag{54a}$$

$$k_0 = k_{0\nu} \left[\frac{J - \Phi_{\mathrm{s}\nu}}{1 - \Phi_{\mathrm{s}\nu}} \right]^{\kappa_0} \exp\left(\tfrac{1}{2} m_0 [J^2 - 1] \right). \tag{54b}$$

The material parameters κ_0 and m_0 as well as the expressions of the volumetric fractions $\Phi_{\mathrm{s}\nu}$, $\Phi_{0\mathrm{s}\nu}$, and $\Phi_{1\mathrm{s}\nu}$ are reported in Table 1.

We solve Eqs. (53a)–(53d) for a cylindric specimen of tissue, of initial height $L = 1\,\mathrm{mm}$ and initial radius $R = 1.5\,\mathrm{mm}$, and whose boundary can be written as $\partial\mathscr{B} = \partial\mathscr{B}_{\mathrm{U}} \sqcup \partial\mathscr{B}_{\mathrm{L}} \sqcup \partial\mathscr{B}_{\ell}$, where the subscripts "U", "L", "ℓ" stand for "upper", "lower" and "lateral", respectively. Then, we complete Eqs. (53a)–(53d) with the following boundary and initial conditions

$$\begin{aligned}
-(\boldsymbol{K}\,\mathrm{Grad}\,p).\boldsymbol{N} &= 0, && \text{on } \partial\mathscr{B}_{\mathrm{U}} \sqcup \partial\mathscr{B}_{\mathrm{L}}, && (55\mathrm{a})\\
p &= 0, && \text{on } \partial\mathscr{B}_{\ell}, && (55\mathrm{b})\\
[\chi(X,0) - \chi(X,t)].\boldsymbol{e}_3 &= u(t), && \text{on } \partial\mathscr{B}_{\mathrm{U}}, && (55\mathrm{c})\\
\chi(X,t) - \chi(X,0) &= \boldsymbol{0}, && \text{on } \partial\mathscr{B}_{\mathrm{L}}, && (55\mathrm{d})\\
\left(-J\,p\,\boldsymbol{g}^{-1}\boldsymbol{F}^{-\mathrm{T}} + \boldsymbol{P}_{\mathrm{sc}}\right).\boldsymbol{N} &= \boldsymbol{0}, && \text{on } \partial\mathscr{B}_{\ell}, && (55\mathrm{e})\\
(\Phi_{1\mathrm{s}\nu} D_0 \boldsymbol{B}_{\mathrm{p}}\,\mathrm{Grad}\,\mathfrak{q}).\boldsymbol{N} &= 0, && \text{on } \partial\mathscr{B}_{\mathrm{U}} \sqcup \partial\mathscr{B}_{\ell}, && (55\mathrm{f})\\
\mathfrak{q}(X,t) &= 0, && \text{on } \partial\mathscr{B}_{\mathrm{L}}, && (55\mathrm{g})\\
\chi(X,0) &= \chi_0(X), && \text{in } \mathscr{B}, && (55\mathrm{h})\\
\mathfrak{q}(X,0) &= \mathfrak{q}_{\mathrm{hist}}(X), && \text{in } \mathscr{B}, && (55\mathrm{i})\\
\boldsymbol{V}(X,0) &= \boldsymbol{G}^{-1}(X), && \text{in } \mathscr{B}. && (55\mathrm{j})
\end{aligned}$$

In (55a), (55e), and (55f), $\boldsymbol{N}$ is the field of unit vectors normal to $\partial\mathscr{B}$; in (55c), the imposed displacement $u(t)$ is given by

$$u(t) = \frac{u_{\max}\,t}{t_{\mathrm{ramp}}}[\Theta(t) - \Theta(t - t_{\mathrm{ramp}})] + u_{\max}\Theta(t - t_{\mathrm{ramp}}), \tag{56}$$

where $\Theta(s) = 1$, for $s \geq 0$, and $\Theta(s) = 0$, for $s < 0$, $u_{\max} = 0.20\,\mathrm{mm}$ is the maximum imposed displacement, and $t_{\mathrm{ramp}} = 20\,\mathrm{s}$ is the final time of the loading ramp. In the simulated compression test, $u_{\max}$ is kept constant until $t_{\mathrm{f}} = 120\,\mathrm{s}$. In (55h), $\chi_0(X)$ represents the initial placement and, in this work, it returns the points X of the reference configuration $\mathscr{B}$. In (55i), $\mathfrak{q}_{\mathrm{hist}}(X)$ denotes the initial distribution of the fibre mean angle, and is taken here to

be equal to an experimentally observed "histological" profile [49], given by

$$\mathfrak{q}_{\mathrm{hist}}(X) = \frac{\pi}{2}\left\{1 - \cos\left(\frac{\pi}{2}\left[-\frac{2}{3}\left(\frac{X^3}{L}\right)^2 + \frac{5}{3}\frac{X^3}{L}\right]\right)\right\}, \tag{57}$$

where X^3 is the axial coordinate. Finally, the initial value $\boldsymbol{V}(X,0)$ is taken in (55j) equal to the inverse metric tensor associated with $\mathscr{B}$, which means that no inelastic distortions occur before the deformation process commences.

We remark that (53a)–(53d) are valid in general, in the sense that they apply to the studied system, under all the specified hypotheses, but without any specialisation to a particular benchmark problem. In fact, they can be adopted for a variety of case studies, and to formulate a proof of concept for testing a proposed model. In our work, we employ (53a)–(53d) for analysing the coupling among fluid flow, deformation and structural reorganisation of the matrix, and fibre reorientation in the tissue under study. For this purpose, we solve numerically a well-documented benchmark test consisting in the unconfined compression of a cylindrical specimen of tissue. The latter is assumed here to be articular cartilage because of the availability of experimental data, but the test can also be performed on other tissues. For the considered test, a sample of tissue is placed between two plates, assumed to be rigid and impermeable (see (55a)), as shown in 2. The lower plate is fixed and the specimen is clamped to it, so as to simulate the adhesion of the cartilage to bone (see (55d)). The upper plate, instead, compresses axially the sample (see (55c)), in such a way that the deformation remains axial-symmetric over the whole duration of the simulation. The lateral surface of the sample is assumed to constitute a free boundary, which means that both the pressure and the radial stress have to be equal to zero (see (55b) and (55e)).

We also have to impose boundary conditions on the fibre mean angle, $\mathfrak{q}$. These are specified by (55f) and (55g). The Dirichlet condition (55g) forces the fibres to remain orthogonal to the bone-cartilage interface for the whole duration of the simulation. Due to the geometry of the specimen and the symmetry of the problem, this restriction implies that, on the lower boundary, the fibres are maintained parallel to the specimen's symmetry axis. Furthermore, the Neumann condition (55f) requires that the normal component of $\boldsymbol{y}^{(1)} = \Phi_{1s\nu} D_0 \boldsymbol{B}_{\mathrm{p}} \mathrm{Grad}\mathfrak{q}$ vanishes on the upper and lateral boundary of the sample. We notice that the coupling between $\mathfrak{q}$ and $\boldsymbol{F}_{\mathrm{p}}$,

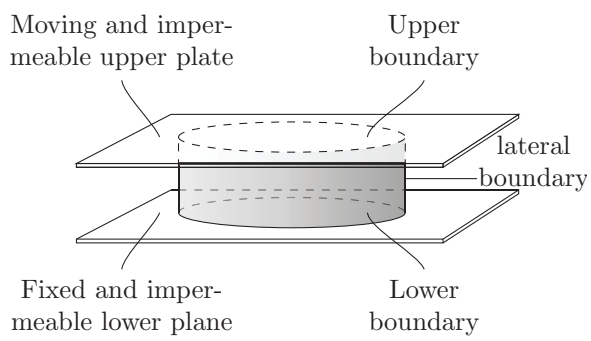

Figure 2: Panel describing the considered benchmark test

accounted for by $\boldsymbol{B}_{\mathrm{p}} = \boldsymbol{F}_{\mathrm{p}}^{-1}.\boldsymbol{F}_{\mathrm{p}}^{-\mathrm{T}}$, affects the way in which (55f) is satisfied and, consequently, the way in which $\mathfrak{q}$ approaches the boundary. Indeed, in the absence of plastic-like distortions, i.e., for $\boldsymbol{B}_{\mathrm{p}} = \boldsymbol{G}^{-1}$, (55f) requires that the normal derivative of $\mathfrak{q}$ is zero on $\partial\mathscr{B}_{\mathrm{U}} \sqcup \partial\mathscr{B}_{\ell}$. For $\boldsymbol{B}_{\mathrm{p}} \neq \boldsymbol{G}^{-1}$, this result is no longer true, and the gradient of $\mathfrak{q}$ is no longer orthogonal to $\boldsymbol{N}$.

Remark 1. *To clarify the physical meaning of* (55f)*, we recall that, in our model,* $\mathfrak{q}$ *and* $\mathrm{Grad}\mathfrak{q}$ *are kinematic descriptors and, consistently with* (3)*, the vector* $\boldsymbol{y}^{(1)}$ *is the internal generalised force conjugated with* $\mathrm{Grad}\mathfrak{q}$*. Thus,* $\boldsymbol{y}^{(1)}$ *plays the role of stress and, as anticipated in* (4b)*,* $\boldsymbol{y}^{(1)}.\boldsymbol{N}$ *is the stress component that has to balance the generalised "contact" force* $h^{(1)}$*, defined on the Neumann boundary of the sample. It follows from these considerations that* (55f) *rephrases* (4b) *in the particular case in which no such forces are active, thereby yielding* $\boldsymbol{y}^{(1)}.\boldsymbol{N} = h^{(1)} = 0$*. This amounts to say that* $\partial\mathscr{B}_{\mathrm{U}} \sqcup \partial\mathscr{B}_{\ell}$ *is a free boundary with respect to* $\mathfrak{q}$*.*

6. Results

To perform a comparative study of the various phenomena accounted for in our work, we consider four different sub-models, which we denominate M1, M2, M3, and M4.

Model M1 (poroelasticity with $\mathscr{R}_{\nu}^{\mathrm{ext}} = 0$*).* As reference case, we consider a deformable porelastic material, in which the evolution of the fibre direction is driven by deformation only. Thus, we solve (53a)–(53c), along with (55a)–(55i). In the computations we set $\mathscr{R}_{\nu}^{\mathrm{ext}}$ equal to zero, which amounts to ignore

in (53c) all the terms containing the target angle $\mathfrak{q}_T$. We do that with the aim of providing an estimate of the importance of the target angle on the guidance of the fibre evolution. Indeed, even in the absence of $\mathscr{R}_\nu^{\text{ext}}$, the inhomogeneity of the fibre mean angle and the generalised forces $\Phi_{1\text{s}\nu}\partial(\hat{W}_{1\text{a}} + \hat{W}_{\text{str}})/\partial\mathfrak{q}$ are capable of triggering the evolution of the fibres. By dealing with a poroelastic model, $\boldsymbol{V}$ is kept equal to its initial value, $\boldsymbol{G}^{-1}$, thereby switching off the evolution of the plastic-like distortions.

Model M2 (poroelasticity with $\mathscr{R}_\nu^{\text{ext}} \neq 0$). This case is the completion of the model M1, as fibre re-orientaion is also driven by the target angle. To this end, we solve the same set of equations and initial and boundary conditions as implemented in M1. In M2, however, all the terms appearing in (53c) are activated, and $\mathfrak{q}_T$ is computed as

$$\begin{aligned}\mathfrak{q}_T &= \arctan\left(\frac{1}{C_{\text{e}33}}\left[\frac{1}{2\pi}\int_0^{2\pi}\boldsymbol{C}_{\text{e}} : \mathfrak{e}_R(\varphi)\otimes\mathfrak{e}_R(\varphi)\text{d}\varphi\right]\right)\\ &= \arctan\left(\frac{\frac{1}{2}[C_{\text{e}11}+C_{\text{e}22}]}{C_{\text{e}33}}\right),\end{aligned} \tag{58}$$

where $\mathfrak{e}_R(\varphi) = \cos\varphi\,\mathfrak{e}_1 + \sin\varphi\,\mathfrak{e}_2$ is a unit vector orthogonal to the specimen's symmetry axis, and oriented radially. Note that other definitions are possible. For example, one may define the target angle as a function of stress [12, 31, 32, 33] or as a function of the deformation [31]. The expression of $\mathfrak{q}_T$ given in (58) takes inspiration from [12, 31], and assumes that the target angle is entirely determined by $\boldsymbol{C}_{\text{e}}$. Specifically, the factor $\frac{1}{2}[C_{\text{e}11} + C_{\text{e}22}]$ is the in-plane directional average of the radial component of $\boldsymbol{C}_{\text{e}}$, while $C_{\text{e}33}$ is the axial component of $\boldsymbol{C}_{\text{e}}$. Under the considered loading conditions, (58) implies that, for increasing radial dilatation and increasing axial contraction, $\frac{1}{2}[C_{\text{e}11} + C_{\text{e}22}]/C_{\text{e}33}$ tends towards infinity, and $\mathfrak{q}_T$ tends towards $\pi/2$. In this limit, the target angle indicates that the fibres should be preferably aligned orthogonally to the specimen's symmetry axis. Clearly, the way in which the fibre mean angle complies with this condition is modulated both by the deformation and the plastic-like distortions. To us, another physically relevant situation occurs in the absence of deformation and elastic distortions, i.e., when (58) prescribes $\mathfrak{q}_T = \pi/4$, and (53c) becomes

$$\Gamma\dot{\mathfrak{q}} = \text{Div}[\Phi_{1\text{s}\nu}D_0\boldsymbol{G}^{-1}\text{Grad}\mathfrak{q}] - \Phi_{1\text{s}\nu}\mathscr{A}_0\frac{\text{d}\mathscr{P}}{\text{d}\mathfrak{q}}. \tag{59}$$

In this case, the concept of target angle $\mathfrak{q}_T$ as manifestation of external force is not explicitly present in (59), and the evolution of $\mathfrak{q}$ is self-driven, with the target angles being identified with the stationary solutions of (59).

Model M3 (full model, with $\mathscr{R}_\nu^{\text{ext}} = 0$). This case study is complete, since it requires to solve the whole set of the model equations (53a)–(53d) together with (55a)–(55g) and (55h)–(55j). However, as done in M1, in the computations we set $\mathscr{R}_\nu^{\text{ext}}$ equal to zero.

Model M4 (full model). As for M3, also M4 describes the complete model and requires the solution of the same list of equations, with the same boundary and initial conditions. However, in M4 the target angle is accounted for.

Computational aspects. To determine the numerical solution of our problem, we perform Finite Element simulations for each of the sub-models M1, M2, M3, and M4. This requires the weak formulation of (53a)–(53d), the generation of a grid for the discretisation of $\mathscr{B}$ and $\partial\mathscr{B}$, and the selection of a time integration scheme. Since the problem is nonlinear, a linearisation procedure is necessary. In general, the grid is unstructured and the interpolations adopted for p, χ, and $\mathfrak{q}$ are different from each other. Equation (53d) is solved only at the integration points of the finite element discretisation, for it does not contain partial derivatives of $\boldsymbol{V}$ with respect to the spatial variables. Hence, we do not provide any weak form for (53d), nor do we introduce in this work test functions associated with $\boldsymbol{V}$.

A Backward Euler scheme of the fifth order is used for the integration in time of all the model equations and boundary conditions. Moreover, in each sub-model, the directional averages of the constitutive functions are computed by employing the Spherical Design Algorithm (see e.g. [14, 58]) as implemented in [15], i.e., the integrals over $\mathbb{S}^2\mathscr{B}$ are evaluated for each time step and at each iteration of the Newton method.

In our work, the numerical simulations were performed with the aid of the commercial software COMSOL©v5.3. Details about the algorithms used for the Finite Element solution of a problem involving (53a), (53b), and an evolution equation similar to (53d) can be found in [29, 59].

Comments to figures. To sample the data, we took four measuring points, located along the vertical axis, and with cartesian coordinates $X_L = (0, 0, L)$, $X_{3L/4} = (0, 0, 3L/4)$, $X_{L/4} = (0, 0, L/4)$, $X_0 = (0, 0, 0)$.

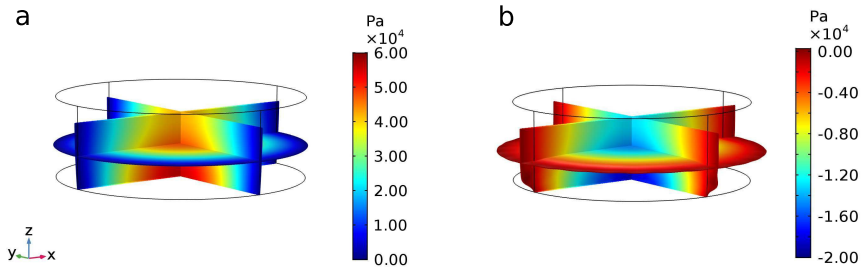

Figure 3: Pressure. 3D contour plots of the pressure for the models M2 (panel a) and M4 (panel b), whilst showing the deformation undergone by the tissue. The models M1 and M3 are not reported since they would lead to no observable difference with respect to M2 and M4, respectively.

First of all, we present a three-dimensional view of the deformed tissue at the end of the loading history. Figure 3 depicts the differences in the deformation of the sample and in the pressure distribution for the models M2 and M4. The radial displacement of the tissue appears relatively contained in M2 (Fig. 3a), while it is more pronounced in M4, i.e., when plastic distortions are active (Fig. 3b). A peculiar characteristic of this case is given by the shape of the profile of the deformed lateral boundary. Indeed, in M2, such profile undergoes a gradual deformation from the bottom to the top, whereas in M4 it experiences an abrupt deformation close to the bottom, while it remains almost parallel to the symmetry axis in the middle and in the upper parts of the sample. A possible explanation of this phenomenon can be outlined through the analysis of the fibre mean angle, as shown in Fig. 5.

Another peculiarity of Fig. 3 concerns the values attained by the pressure. In contrast to the elastic case, when plastic-like distortions are accounted for, the pressure goes lower than zero, thereby leading to a "syringe effect" [25]. To better describe this phenomenon, Fig. 4 presents the time variation of the pressure in X_0. No significant differences can be observed for models M1 and M2, in which, after the increase due to the loading ramp, the pressure monotonically decreases toward zero. On the other hand, for both models accounting for the plastic-like distortions, i.e., M3 and M4, after a first rapid increase at the beginning of the loading experiment, we observed a rather slow increase of the pressure values. Afterwards, when the loading ramp terminates, we assist to an abrupt pressure drop, that leads to negative pressure values. This sudden change is then followed by a slow recovery, that would lead to null pressure in the long term.

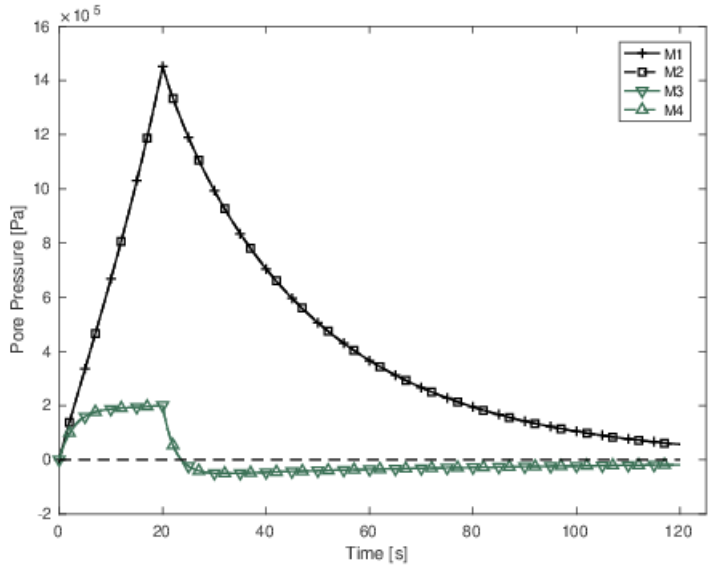

Figure 4: Time-evolution of the pore pressure. For all the implemented models, the temporal evolution of the pore pressure is monitored in X_0.

A key point of this work is the role played by the fibre mean angle and by the target angle. To analyse their evolution we present Fig. 5. The top panels of Fig. 5 depict the evolution of the fibre mean angle, $\mathfrak{q}$, along the symmetry axis, starting from the initial histological profile (55i), to the final fibre distribution obtained within M2 (Fig. 5a) and M4 (Fig. 5b). Note that, thanks to the upper boundary condition 55f, the value of $\mathfrak{q}$ corresponding to the upper surface is free to evolve. Interestingly, the greater variations are registered in the plastic case (M4) and, enhanced by the introduction of the gradient term, the variability extends to the tissue beneath. While in the middle-upper portion of the tissue we assist to a smooth change of the fibre mean angle, on the lower part there is quite an abrupt variation from the histological profile. This might be due to the Dirichlet boundary condition on the lower boundary of the specimen.

To understand the role of $\mathfrak{q}_T$ and to further describe the behaviour of $\mathfrak{q}$, the temporal evolution of the fibre mean angle is shown in the lower panels of Fig. 5, where the trend of the target angle $\mathfrak{q}_T$ is presented alongside the fibre mean angle, evaluated in two different sampling points. Indeed, by comparing M1 with M2, and M3 with M4, it is evident that the introduction

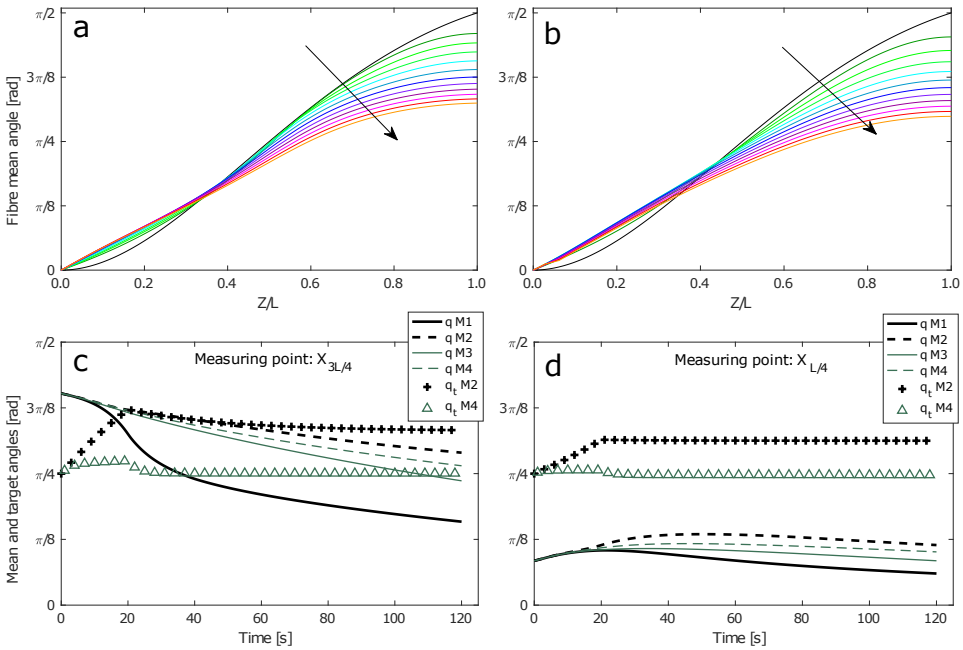

Figure 5: Fibre mean angle. In panels a and b, 10 seconds time-laps recording the evolution of the fibre mean angle along the vertical axis, for M2 (a) and M4 (b); arrows indicate the increase of time. In panels c and d, the temporal evolution of both the fibre mean angle and the target angle, observed in $X_{3L/4}$ (c) and $X_{L/4}$ (d), for all the presented models. The target angle is implemented in M2 and M4 only.

of $\mathfrak{q}_T$ strongly modulates $\mathfrak{q}$ by controlling, and then by reducing, its variation, especially in M2. In particular, looking at Fig. 5d, we see how $\mathfrak{q}$ is driven upward by the presence of $\mathfrak{q}_T$ (M2 and M4), especially during the loading ramp.

Comparing Fig. 3 with Fig. 5c and Fig. 5d, we notice that the behaviour of $\mathfrak{q}$ influences the way in which the tissue deforms. Indeed, the more the variation of $\mathfrak{q}$ is contained in time, the less the sample tends to deform radially. This behaviour is model dependent and is more evident for M3 end M4 than it is for M1 and M2.

The analysis of the target angle is worth of a separate discussion. Once again, by making reference to Fig. 5c and Fig. 5d there are appreciable differences among the elastic and the plastic case studies, concerning both the evolution and the stationary limit of $\mathfrak{q}_T$. The most relevant variations of $\mathfrak{q}_T$ can be appreciated in M2, in which the relatively high values of the target

angle, reached at the end of the loading ramp, seem to affect the stationary limit. In this case, different values of $\mathfrak{q}_T^\infty$ are recovered at a different depth. On the other hand, in M4 elastic distortions fade after the loading ramp, practically leading to the recovery of the stationary value $\pi/4$ throughout the whole tissue.

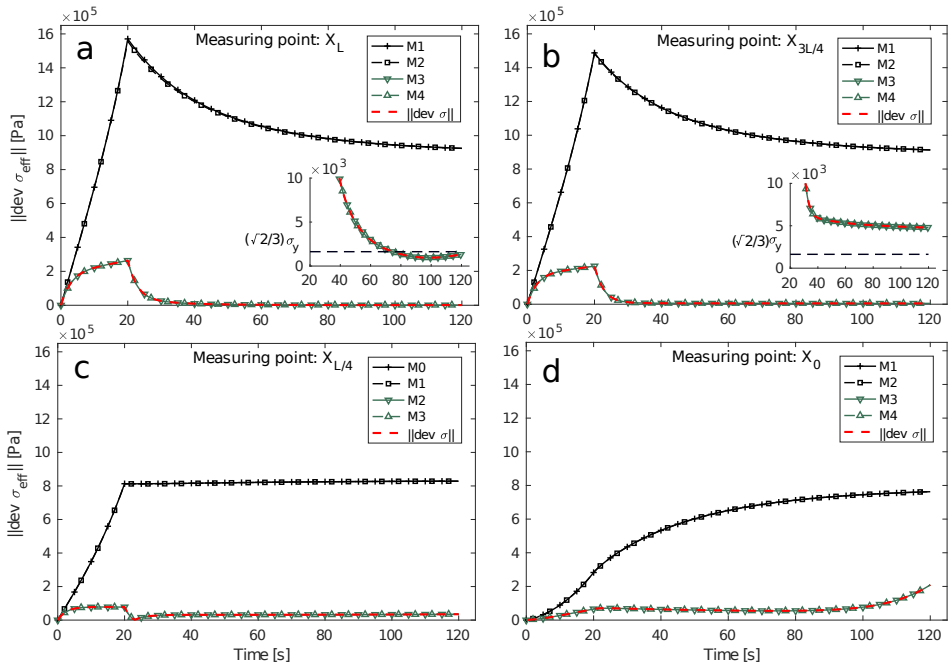

Figure 6: Effective stress tensor. For all the presented models, the norm of the effective stress tensor is evaluated in the measuring points X_L (a), $X_{3L/4}$ (b), $X_{L/4}$ (c) and X_0 (d).

To complete the analysis, Fig. 6 depicts the norm of the deviatoric part of the effective stress tensor, i.e., $\|\mathrm{dev}\boldsymbol{\sigma}_{\mathrm{eff}}\|_{\boldsymbol{g}}$. With the exception of the bottom of the sample (see Fig. 6d), where the specimen is tied to the tidemark, $\|\mathrm{dev}\boldsymbol{\sigma}_{\mathrm{eff}}\|_{\boldsymbol{g}}$ reaches its maximum at the end of the loading ramp. The consequent decrease towards a stationary value is monotonic for the elastic cases M1 and M2, while it is not for the plastic models M3 and M4 (see Figs. 6a and 6c). In the insert of Figs. 6a and 6b, $\sqrt{2/3}\sigma_y$ is reported to highlight when and where plastic-like distortions are de-activated. In Fig. 6a we note that, after approximately 70 s, the effective stress is below the threshold $\sqrt{2/3}\sigma_y$, thereby implying a temporary switch-off of the plastic-like distortions. Figure 6 also reports $\|\mathrm{dev}\boldsymbol{\sigma}\|_{\boldsymbol{g}}$, evaluated for model M4. Although not

visible at the length scale selected for our figures, we do measure differences between the effective stress, $\boldsymbol{\sigma}_{\mathrm{eff}}$, and the "standard" Cauchy stress $\boldsymbol{\sigma}$, which does not take into account $\boldsymbol{\Sigma}_{\mathrm{Grad}}$. In turn, $\boldsymbol{\Sigma}_{\mathrm{Grad}}$ is influenced by $\Phi_{1\mathrm{s}\nu}$ and $\boldsymbol{B}_{\mathrm{p}}$, and it vanishes gradually on the way to X_L, because of the Neumann zero boundary condition on $\mathfrak{q}$ on $\partial\mathscr{B}_{\mathrm{U}}$.

7. Discussion

The key aspect of our work is the mutual interaction among the motion, χ, the tensor of plastic-like distortions, $\boldsymbol{F}_{\mathrm{p}}$, and the fibre mean angle, $\mathfrak{q}$. Firstly, we notice that $\boldsymbol{F}_{\mathrm{p}}$ and $\mathfrak{q}$ interact with χ through the constitutive law expressing $\boldsymbol{P}_{\mathrm{sc}}$ in (53b). Secondly, χ and $\mathfrak{q}$ interact with $\boldsymbol{F}_{\mathrm{p}}$ through the term between parentheses in (53d). Such interaction manifests itself through $\boldsymbol{C}$ and $\boldsymbol{\Sigma}_{\mathrm{eff}}$. Thirdly, the interaction of χ and $\boldsymbol{F}_{\mathrm{p}}$ with $\mathfrak{q}$ finds its expression in the generalised forces $\Phi_{1\mathrm{s}\nu}[\partial(\hat{W}_{1\mathrm{a}} + \hat{W}_{\mathrm{str}})/\partial\mathfrak{q}]$. Finally, $\boldsymbol{F}_{\mathrm{p}}$ and $\mathfrak{q}$ interact with each other through $\Phi_{1\mathrm{s}\nu} D_0 \boldsymbol{B}_{\mathrm{p}} \mathrm{Grad}\,\mathfrak{q}$, i.e., in such a way that only two players out of three interact.

Role played by the free energy density W_{Grad}. In the form given in (19), W_{Grad} constitutes the lowest-order approximation of the self-interaction of the scalar field $\mathfrak{q}$. The strength of such self-interaction is measured by D_0. As in [24], we consider the particular case in which $\hat{W}_{\mathrm{Grad}}$ is independent of deformation, but we do allow it to depend on the plastic-like distortions through $\boldsymbol{B}_{\mathrm{p}}$, whose presence generates $\boldsymbol{\Sigma}_{\mathrm{Grad}}$. This tensor is purely configurational, and has no direct geometric counterpart, since it emerges as a consequence of the coupling between the structural degrees of freedom $\mathfrak{q}$ and $\boldsymbol{F}_{\mathrm{p}}$. More importantly, $\boldsymbol{\Sigma}_{\mathrm{Grad}}$ features as a summand of $\boldsymbol{\Sigma}_{\mathrm{eff}}$ among the configurational forces that drive the evolution law of the plastic-like distortions in (52). Hence, differently from other models on the subject (see e.g. [33]), in which the configurational stress that triggers remodelling can be obtained from Cauchy stress, in our theory we have the configurational force $\boldsymbol{\Sigma}_{\mathrm{Grad}}$ that exists on its own, and participates to activate the structural reorganisations of the tissue. In fact, it might be interpreted as the contribution to the structural reorganisation given by the reorientation of the fibres, i.e., the output of the interplay between $\boldsymbol{F}_{\mathrm{p}}$ and $\mathfrak{q}$ alone.

Role played by the free energy density W_{str}. The energy density W_{str} defined in our model is such that the "structural" contribution to the overall second

Piola-Kirchhoff stress tensor, $\boldsymbol{S}_{\rm str} = 2\Phi_{1s\nu}(\partial\hat{W}_{\rm str}/\partial\boldsymbol{C}_{\rm e})$, and the "structural" contribution to the overall elasticity tensor, $\mathbb{C}_{\rm str} = 4(\partial^2\hat{W}_{\rm str}/\partial\boldsymbol{C}_{\rm e}^2)$ vanishes in the natural state. The function $\mathscr{A}_0\mathscr{P}(\mathfrak{q})$ coincides with the structural energy in the natural state, i.e., $\hat{W}^{(0)}_{\rm str}(\mathfrak{q}) = \mathscr{A}_0\mathscr{P}(\mathfrak{q})$. We notice that such functional form is adequate for describing large fluctuations of the order parameter $\mathfrak{q}$ from the two reference values $\mathfrak{q}_0 = 0$ and $\mathfrak{q}_1 = \pi/2$, each of which returns the global minimum of $\hat{W}^{(0)}_{\rm str}$, i.e., $\hat{W}^{(0)}_{\rm str}(0) = \hat{W}^{(0)}_{\rm str}(\pi/2) = 0$. As discussed in [24], an example of this behaviour is provided by the articular cartilage used for mechanical tests [49] in which, prior to the application of any loading history, a "histological profile" of the fibre mean angle can be defined [24, 49], which varies throughout the tissue, taking on the values $\mathfrak{q}_0$ and $\mathfrak{q}_1$ at the interface with the bone and at the articular surface, respectively (see e.g. [60]).

One may wonder whether the introduction of $W_{\rm str}$ is really necessary and, if it is, why it should have the functional form suggested in this work. To answer these questions, let us first notice that there are studies in which the structural energy is tacitly used. Baaijens et al. [31], for example, prescribe that the fibre mean angle evolves according to the law

$$\dot{\mathfrak{q}} = -\tfrac{1}{\tau}[\mathfrak{q} - \mathfrak{q}_T], \tag{60}$$

where τ is a model parameter describing the system's relaxation coefficient, $\mathfrak{q}$ is the angle that the fibres in a blood vessel form with the symmetry axis, and the target angle, $\mathfrak{q}_T$, determines the preferred alignment of the fibres (in the case of a blood vessel, $2\mathfrak{q}$ is the angle between the two families of fibres coiled helically around the vessel). Looking at (60), and comparing it with our (46), which is obtained in the limit of vanishing D_0, we notice that (60) can be recovered from (46) by neglecting the force $\Phi_{1s\nu}(\partial\hat{W}_{1\rm a}/\partial\mathfrak{q})$, and retaining only $\Phi_{1s\nu}(\partial\hat{W}_{\rm str}/\partial\mathfrak{q})$, with the constitutive choice

$$\hat{W}_{\rm str}(\mathfrak{q}) \equiv \hat{W}^{\rm quad}_{\rm str}(\mathfrak{q}) = \tfrac{1}{2}\kappa[\mathfrak{q} - \mathfrak{q}_{\rm ref}]^2, \tag{61}$$

where the superscript "quad" stands for "quadratic", κ is an angular stiffness density (thus, having units of force per unit area), and $\mathfrak{q}_{\rm ref}$ is a reference angle. Indeed, computing the derivative of $\hat{W}^{\rm quad}_{\rm str}$ with respect to $\mathfrak{q}$, and substituting the result into (46) yield

$$\Gamma\dot{\mathfrak{q}} = -\Phi_{1s\nu}\kappa[\mathfrak{q} - \mathfrak{q}_T], \tag{62}$$

and (60) is re-obtained upon identifying $1/\tau = \Phi_{1s\nu}\kappa/\Gamma$.

In the absence of deformation and plastic-like distortions, $W_{\rm std}$ vanishes identically, regardless of the value taken by $\mathfrak{q}$, and the energetic content of the tissue is the integral over $\mathscr{B}$ of the remodelling energy density

$$\hat{W}^{(0)}_{\rm rem}(\mathfrak{q}, {\rm Grad}\mathfrak{q}) = \tfrac{1}{2}\Phi_{1s\nu}D_0\|{\rm Grad}\mathfrak{q}\|^2 + \Phi_{1s\nu}\hat{W}^{(0)}_{\rm str}(\mathfrak{q}), \tag{63}$$

which is nonzero for $\mathfrak{q}$ other than the constant values $\mathfrak{q} = \mathfrak{q}_0$ and $\mathfrak{q} = \mathfrak{q}_1$ [24]. Hence, as reported in [24], the "natural state" of the tissue, which corresponds to the state of zero mechanical stress, is not necessarily its *ground state*, which is attained when the residual energy density $\hat{W}^{(0)}_{\rm rem}$ reaches its global minimum. The ground state, in fact, is individuated by either $\mathfrak{q} = \mathfrak{q}_0$ or $\mathfrak{q} = \mathfrak{q}_1$, for which each term on the right-hand-side of (63) is identically null. In our case, the probability density, $\check{\Psi}(\vartheta, \mathfrak{q}_0)$, depicts the situation in which the fibres are most likely oriented along the tissue's symmetry axis, whereas $\check{\Psi}(\vartheta, \mathfrak{q}_1)$ describes the case in which the fibres tend to align themselves perpendicularly to the symmetry axis. Any other distribution of the fibre mean angle corresponds to a deviation from the ground state, and is associated with nontrivial energies. The coefficient $\mathscr{A}_0$ defines the height of the energy barrier that has to be overcome to pass from one ground state configuration, e.g. $\mathfrak{q}_0$, to the other one, $\mathfrak{q}_1$, or vice versa. In our model, such height is assumed to depend only on $\Phi_{1s\nu}$, which is point-dependent. However, when deformation and plastic-like distortions are active, we allow for a modulation of $\mathscr{A}_0$ by means of the terms between brackets in (17). Note that, since the directional average in (17) depends on $\mathfrak{q}$, the modulation also represents a self-interaction of the fibre-mean angle.

8. Conclusions

We proposed two conceptual results that, to the best of our knowledge, might be regarded as novelties: First, our calculations naturally lead to a Mandel-like stress tensor, denoted by $\boldsymbol{\Sigma}_{\rm Grad}$, which contributes to the onset and evolution of the plastic-like distortions. These, in turn, contribute to the evolution of the fibre mean angle through the term $\Phi_{1s\nu}D_0\boldsymbol{B}_{\rm p}{\rm Grad}\mathfrak{q}$. Secondly, we define a structural energy that generalises some other choices available in the literature (see e.g. [31]). These results, discussed in detail in Sect. 7, characterise the interplay between the reorientation of fibres and plastic-like distortions.

As anticipated in Sect. 2, our model can be used, with some modifications, for a generic tissue with fibre-reinforcement and evolving internal structure. The major strength of our model is its flexibility, since it establishes the "mathematical infrastructure" for describing transverse isotropy and for resolving interactions that are usually not resolved in more "classical" theories (see e.g. [31, 33, 40]). In turn, its major weakness is that it does not account for growth, which is crucial for tissues like cellular aggregates and tumours.

Describing growth requires to reformulate the present setting to consider different cell populations, include chemical substances, and account for the coupling among stress, structural reorganisation, and variation of mass. These modifications result in the introduction of an evolution equation for the inelastic distortions related to growth, and in one mass balance law for each chemical species and cell population considered in the model. All these equations should be combined with (53a)–(53d), and new interactions should be resolved. These also call for a review of the constitutive framework.

Another possible specific problem for which our theory could be useful is "inverse poroelasticity" [61]. Finally, the theory presented in this work could be compared with that developed by Capriz in [62], and this is subject of our current investigations.

Conflict of interest

The Authors declare that they have no conflict of interest.

Acknowledgments

Our warmest thanks go to Salvatore Federico (The University of Calgary, Canada), co-author of the paper from which the present work originates [24], for the uncountable scientific discussions and the invaluable help all through the years; to Prof. Gaetano Giaquinta (1945–2016), who first suggested the idea of working with free energy densities of the Ginzburg-Landau type; and to Prof. Marcelo Epstein (The University of Calgary, Canada) for his precious suggestions, especially concerning the literature. His depth of thought has helped us improve our work. Finally, EC and AG thank the *Dipartimento di Scienze Matematiche* (DISMA) "G.L. Lagrange" of the *Politecnico di Torino* for financial support.

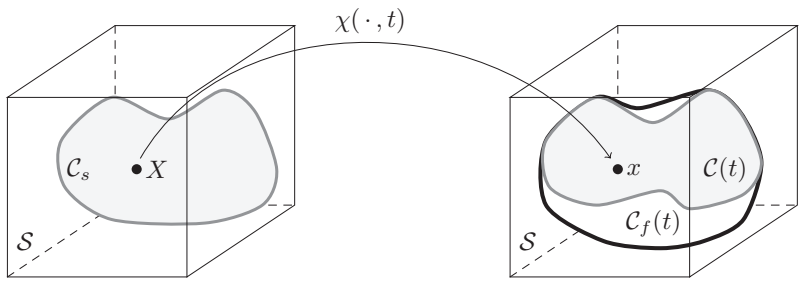

Figure 7: Schematic representation of the considered kinematics of mixtures.

Appendix

We recall some concepts of the kinematics of biphasic mixtures. To this end, we adopt the theory put forward in [63], and used in [15, 24, 29, 45]. Accordingly, the set $\mathscr{B} \subset \mathscr{S}$ is introduced as the reference placement of the solid. Then, $\chi : \mathscr{B} \times \mathscr{I} \to \mathscr{S}$ denotes a smooth mapping such that $\mathscr{C}_{\mathrm{s}}(t) \equiv \chi(\mathscr{B}, t) \subset \mathscr{S}$ is the configuration of the solid at time $t \in \mathscr{I}$, and $\mathscr{C}_{\mathrm{f}}(t)$ is the portion of $\mathscr{S}$ occupied by the fluid at the same instant of time. Finally, $\mathscr{C}(t) := \mathscr{C}_{\mathrm{s}}(t) \cap \mathscr{C}_{\mathrm{f}}(t) \subset \mathscr{S}$ is the region of space in which the solid-fluid mixture finds itself at $t \in \mathscr{S}$. Even though $\chi(\,\cdot\,,t) : \mathscr{B} \to \mathscr{S}$ is not invertible, the map $\hat{\chi}(\,\cdot\,,t) : \mathscr{B} \to \mathscr{C}_{\mathrm{s}}(t)$, defined by $\hat{\chi}(X,t) = \chi(X,t)$ for all $(X,t) \in \mathscr{B} \times \mathscr{I}$, is invertible and such that $\mathscr{B} = \hat{\chi}^{-1}(\mathscr{C}_{\mathrm{s}}(t), t)$. In general, it occurs that $\hat{\chi}^{-1}(\mathscr{C}(t), t) \subset \mathscr{B}$. However, in all the cases studied in our work, the stronger condition $\hat{\chi}^{-1}(\mathscr{C}(t), t) = \mathscr{B}$ applies, since the identity $\mathscr{C}_{\mathrm{s}}(t) = \mathscr{C}(t)$ is verified for all $t \in \mathscr{I}$ see Fig. 7. For this reason, in Eqs. (1a) and (1b), $\mathscr{B}$ can be viewed as a reference placement for the mixture as a whole. We denote by $T_X\mathscr{B}$ and $T_x\mathscr{S}$ the tangent spaces attached to $X \in \mathscr{B}$ and $x \in \mathscr{S}$, respectively [35], and we identify the deformation gradient tensor of the solid with the tangent map of χ, i.e., $\boldsymbol{F}(X,t) : T_X\mathscr{B} \to T_x\mathscr{S}$, with $x = \chi(X,t)$. We also introduce the spatial velocity of the solid at $\chi(X,t) \in \mathscr{C}_{\mathrm{s}}(t)$, ${}^{\mathrm{s}}\boldsymbol{v}_{\mathrm{s}}(\chi(X,t),t)$, and the spatial velocity of the fluid at $x \in \mathscr{C}_{\mathrm{f}}$, ${}^{\mathrm{s}}\boldsymbol{v}_{\mathrm{f}}(x,t)$. In addition, we define the solid velocity field over $\mathscr{B}$, i.e., $\boldsymbol{v}_{\mathrm{s}}(\,\cdot\,,t) : \mathscr{B} \to T\mathscr{S} = \sqcup_{x \in \mathscr{S}} T_x\mathscr{S}$, through $\boldsymbol{v}_{\mathrm{s}}(X,t) := {}^{\mathrm{s}}\boldsymbol{v}_{\mathrm{s}}(x,t)$. For $x \in \mathscr{C}(t) = \mathscr{C}_{\mathrm{s}}(t) \cap \mathscr{C}_{\mathrm{f}}(t)$, there exists $X \in \hat{\chi}^{-1}(\mathscr{C}(t), t)$ such that the equality ${}^{\mathrm{s}}\boldsymbol{v}_{\mathrm{f}}(x,t) = \boldsymbol{v}_{\mathrm{f}}(X,t)$ is verified, thereby defining the fluid velocity field over $\hat{\chi}^{-1}(\mathscr{C}(t), t) \subset \mathscr{B}$, i.e., $\boldsymbol{v}_{\mathrm{f}}(\,\cdot\,,t) : \hat{\chi}^{-1}(\mathscr{C}(t), t) \to T\mathscr{S}$.

With each $x \in \mathscr{C}(t)$ we associate the spatial *volumetric fractions* ${}^{\mathrm{s}}\phi_{\mathrm{s}}(x,t)$ and ${}^{\mathrm{s}}\phi_{\mathrm{f}}(x,t)$, which measure, respectively, the local volumetric content of

solid and fluid with respect to a representative volume of the mixture. Since the mixture is assumed to be saturated, it holds that ${}^{\mathrm{s}}\phi_{\mathrm{s}}(x,t)+{}^{\mathrm{s}}\phi_{\mathrm{f}}(x,t)=1$, for all $x \in \mathscr{C}(t)$ and for all t. Along with ${}^{\mathrm{s}}\phi_{\mathrm{s}}$ and ${}^{\mathrm{s}}\phi_{\mathrm{f}}$, we also introduce $\phi_{\mathrm{s}}(X,t)={}^{\mathrm{s}}\phi_{\mathrm{s}}(\chi(X,t),t)$ and $\phi_{\mathrm{f}}(X,t)={}^{\mathrm{s}}\phi_{\mathrm{f}}(\chi(X,t),t)$, for $X \in \hat{\chi}^{-1}(\mathscr{C}(t),t)$.

Article information

DOI: 10.1016/j.ijnonlinmec.2018.08.022. Available online: November 14, 2018
Journal: *International Journal of Non-Linear Mechanics* 111 (2019) 1-13

References

[1] G. Holzapfel, R. Ogden, On fiber dispersion models: Exclusion of compressed fibers and spurious model comparisons, J. Elast. 129(1-2) (2017) 49–68. doi:10.1007/s10659-016-9605-2.

[2] J. Merodio, On constitutive equations for fiber-reinforced nonlinearly viscoelastic solids, Mech. Res. Commun. 33 (2006) 764–770. doi:10.1016/j.mechrescom.2006.03.009.

[3] M. Vasta, A. Gizzi, A. Pandolfi, On three- and two-dimensional fiber distributed models of biological tissues, Probabilist. Eng. Mech. 37 (2014) 170–179. doi:http://dx.doi.org/10.1016/j.probengmech.2014.05.003.

[4] A. Melnik, H.B. Da Rocha, A. Goriely, On the modeling of fiber dispersion in fiber-reinforced elastic materials, Int. J. Nonlinear Mech. 75 (2015) 92–106. doi:http://dx.doi.org/10.1016/j.ijnonlinmec.2014.10.006.

[5] T. Quinn, V. Morel, Microstructural modeling of collagen network mechanics and interactions with the proteoglycans gel in articular cartilage, Biomech. Model. Mechanobiol. 6 (2007) 73–82. doi:10.1007/s10237-006-0036-z.

[6] S. Federico, W. Herzog, On the anisotropy and inhomogeneity of permeability in articular cartilage, Biomech. Model. Mechanobiol. 7 (2008) 367–378. doi:10.1007/s10237-007-0091-0.

[7] S. Federico, W. Herzog, Towards an analytical model of soft biological tissues, J. Biomech. 41 (2008) 3309–3313. doi:https://doi.org/10.1016/j.jbiomech.2008.05.039.

[8] S. Federico, W. Herzog, On the permeability of fibre-reinforced porous materials, Int. J. Solids Struct. 45 (2008) 2160–2172. doi:https://doi.org/10.1016/j.ijsolstr.2007.11.014.

[9] S. Federico, A. Grillo, Elasticity and permeability of porous fibre-reinforced materials under large deformations, Mech. Mater. 44 (2012) 58–71. doi:10.1016/j.mechmat.2011.07.010.

[10] D. Pierce, T. Ricken, G. Holzapfel, A hyperelastic biphasic fibre-reinforced model of articular cartilage considering distributed collagen fibre orientations: continuum basis, computational aspects and applications, Comput. Methods Biomech. Biomed. Eng. 16 (2013) 1344–1361. doi:10.1080/10255842.2012.670854.

[11] D. Pierce, M. Unterberger, W. Trobin, T. Ricken, G. Holzapfel, A microstructurally based continuum model of cartilage viscoelasticity and permeability incorporating measured statistical fiber orientations, Biomech. Model. Mechanobiol. 15 (2016) 229–244. doi:10.1007/s10237-015-0685-x.

[12] N. Driessen, W. Wilson, C. Bouten, F. Baaijens, A computational model for collagen fibre remodelling in the arterial wall, J. Theor. Biol. 226 (2004) 53–64. doi:10.1016/j.jtbi.2003.08.004.

[13] W. Wilson, N. Driessen, C.C. van Donkelaar, K. Ito, Prediction of collagen orientation in articular cartilage by a collagen remodeling algorithm, Osteoarthr. Cartil. 14 (2006) 1196–1202. doi:10.1016/j.joca.2006.05.006.

[14] S. Federico, T. Gasser, Non-linear elasticity of biological tissues with statistical fibre orientation, J. R. Soc. Interface 7 (2010) 955–966. doi:10.1098/rsif.2009.0502.

[15] M. Carfagna, A. Grillo, The spherical design algorithm in the numerical simulation of biological tissues with statistical fibre-reinforcement, Comput. Vis. Sci. 18 (2017) 157–184. doi:10.1007/s00791-017-0278-6.

[16] K. Hashlamoun, A. Grillo, S. Federico, Efficient evaluation of the material response of tissues reinforced by statistically oriented fibres, Z. Angew. Math. Phys. 67 (2016) 113–145. doi:10.1007/s10237-006-0049-7.

[17] K. Hashlamoun, S. Federico, Transversely isotropic higher-order averaged structure tensors, Z. Angew. Math. Phys. 68(4) (2017) 113–145. doi:10.1007/s00033-017-0830-8.

[18] B. Loret, F.M.F. Simões, A framework for deformation, generalized diffusion, mass transfer and growth in multi-species multi-phase biological tissues, Eur. J. Mech. A 24 (2005) 757–781. doi:10.1016/j.euromechsol.2005.05.005.

[19] W. Lin, M. Iafrati, R. Peattie, L. Dorfmann, Growth and remodeling with application to abdominal aortic aneurysms, J. Eng. Math. In press (2017) 1–25. doi:https://doi.org/10.1007/s10665-017-9915-9.

[20] M. Epstein, G. Maugin, Thermomechanics of volumetric growth in uniform bodies, Int. J. Plasticity 16 (2000) 951–978.

[21] K. Garikipati, E. Arruda, K. Grosh, H. Narayanan, S. Calve, A continuum treatment of growth in biological tissue: the coupling of mass transport and mechanics, J. Mech. Phys. Solids 52 (2004) 1595–1625. doi:10.1016/j.jmps.2004.01.004.

[22] D. Ambrosi, G. Athesian, E. Arruda, et al., Perspectives on biological growth and remodeling, J. Mech. Phys. Solids 59(4) (2011) 863–883. doi:10.1016/j.jmps.2010.12.011.

[23] W. Wilson, J. Huyghe, C.C. van Donkelaar, A composition-based cartilage model for the assessment of compositional changes during cartilage damage and adaptation, Osteoarthr. Cartil. 14 (2006) 554–560. doi:10.1016/j.joca.2005.12.006.

[24] A. Grillo, M. Carfagna, S. Federico, An Allen-Cahn approach to the remodelling of fibre-reinforced anisotropic materials, J. Eng. Math. In Press (2017) 1–34. doi:10.1007/s10665-017-9940-8.

[25] S. Di Stefano, M. Carfagna, M. Knodel, K. Hashlamoun, S. Federico, A. Grillo, Anelastic reorganisation of fibre-reinforced biological tissues, Submitted (2017) 1–16.

[26] D. Garcia, P. Zysset, M. Charlebois, A. Curnier, A three-dimensional elastic plastic damage constitutive law for bone tissue, Biomech. Model. Mechanobiol. 8(2) (2009) 149–165. doi:10.1007/s10237-008-0125-2.

[27] L. Preziosi, D. Ambrosi, C. Verdier, An elasto-visco-plastic model of cell aggregates, J. Theor. Biol. 262(1) (2010) 35–47. doi:10.1016/j.jtbi.2009.08.023.

[28] C. Giverso, L. Preziosi, Modelling the compression and reorganization of cell aggregates, Math. Med. Biol. 29(2) (2012) 181–204. doi:10.1093/imammb/dqr008.

[29] A. Grillo, R. Prohl, G. Wittum, A poroplastic model of structural reorganisation in porous media of biomechanical interest, Continuum Mech. Therm. 28 (2016) 579–601. doi:10.1007/s00161-015-0465-y.

[30] J. Merodio, R. Ogden, J. Rodríguez, The influence of residual stress on finite deformation elastic response, Int. J. Nonliner Mech. 56 (2013) 43–49. doi:10.1016/j.ijnonlinmec.2013.02.010.

[31] F. Baaijens, C. Bouten, N. Driessen, Modeling cartilage remodeling, J. Biomech. 43 (2010) 166–175. doi:10.1016/j.jbiomech.2009.09.022.

[32] I. Hariton, G. de Botton, T. Gasser, G. Holzapfel, Stress-driven collagen fiber remodeling in arterial walls, Biomech. Model. Mechanobiol. 6(3) (2007) 163–175. doi:10.1007/s10237-006-0049-7.

[33] T. Olsson, A. Klarbring, Residual stresses in soft tissue as a consequence of growth and remodeling: application to an arterial geometry, Eur. J. Mech. A 27(6) (2008) 959–974. doi:10.1016/j.euromechsol.2007.12.006.

[34] A. DiCarlo, S. Quiligotti, Growth and balance, Mech. Res. Commun. (2002) 449–456.

[35] J. Marsden, T. Hughes, Mathematical Foundations of Elasticity, Dover Publications, Inc., Mineola, New York, 1983.

[36] P. Cermelli, E. Fried, S. Sellers, Configurational stress, yield and flow in rate-independent plasticity, Proc. R. Soc. Lond. A 457 (2001) 1447–1467. doi:10.1098/rspa.2001.0786.

[37] M. Mićunović, Thermomechanics of Viscoplasticity—Fundamentals and Applications, Springer, Heidelberg, Germany, 2009.

[38] A. Goriely, The Mathematics and Mechanics of Biological Growth, Springer New York, 2016. doi:10.1007/978-0-387-87710-5.

[39] S. Di Stefano, A. Ramírez-Torres, R. Penta, A. Grillo, Self-induced growth through evolving material inhomogeneities, Int. J. Nonlinear Mechanics Submitted.

[40] A. Grillo, G. Wittum, A. Tomic, S. Federico, Remodelling in statistically oriented fibre-reinforced materials and biological tissues, Math. Mech. Solids 20(9) (2015) 1107–1129. doi:10.1177/1081286513515265.

[41] M. Holmes, V. Mow, The nonlinear characteristics of soft gels and hydrated connective tissues in ultrafiltration, J. Biomech. 23 (1990) 1145–1156.

[42] W. Ehlers, B. Markert, A linear viscoelastic biphasic model for soft tissues based on the theory of porous media, Transactions of the ASME 123 (2001) 418–424. doi:10.1115/1.1388292.

[43] Y. Lanir, Constitutive equations for fibrous connective tissues, J. Biomech. 16 (1983) 1–12.

[44] T. Gasser, R. Ogden, G. Holzapfel, Hyperelastic modelling of arterial layers with distributed collagen fibre orientations, J. R. Soc. Interface 3 (2006) 15–35. doi:10.1098/rsif.2005.0073.

[45] A. Tomic, A. Grillo, S. Federico, Poroelastic materials reinforced by statistically oriented fibres — numerical implementation and application to articular cartilage, IMA J. Appl. Math. 79 (2014) 1027–1059. doi:10.1093/imamat/hxu039.

[46] G. Holzapfel, T. Gasser, R. Ogden, A new constitutive framework for arterial wall mechanics and a comparative study of material models, J. Elast. 61(1-3) (2000) 1–48.

[47] M. Destrade, B. M. Donald, J. Murphy, G. Saccomandi, At least three invariants are necessary to model the mechanical response of incompressible, transversely isotropic materials, Comput. Mech. 52 (2013) 959–969. doi:10.1007/s00466-013-0857-4.

[48] M. E. Hamdaoui, J. Merodio, R. Ogden, J. Rodríguez, Finite elastic deformations of transversely isotropic circular cylindrical tubes, Int. J. Nonlinear Mech. 51 (2014) 1188–1196.

[49] S. Federico, A. Grillo, G. L. Rosa, G. Giaquinta, W. Herzog, A transversely isotropic, transversely homogeneous microstructural-statistical model of articular cartilage, J. Biomech. 38 (2005) 2008–2018. doi:10.1016/j.jbiomech.2004.09.020.

[50] A. Grillo, S. Federico, G. Wittum, Growth, mass transfer, and remodeling in fiber-reinforced, multi-constituent materials, Int. J. Nonlinear Mech. 47 (2012) 388–401. doi:10.1016/j.ijnonlinmec.2011.09.026.

[51] G. Maugin, M. Epstein, Geometrical material structure of elastoplasticity, Int. J. Plasticity 14(1-3) (1998) 109–115.

[52] S. Hassanizadeh, Derivation of basic equations of mass transp. porous med., part 2. generalized darcy's and fick's laws, Adv. Water Resour. 9 (1986) 207–222.

[53] L. Schreyer Bennethum, M. Murad, J. Cushman, Macroscale thermodynamics and the chemical potential for swelling porous media, Transp. Porous Med. 39 (2010) 187–225.

[54] M. Gurtin, E. Fried, L. Anand, The Mechanics and Thermodynamics of Continua, Cambridge University Press, 2010.

[55] J. Simo, T. Hughes, Computational Inelasticity, Springer, New York, 1998.

[56] M. Gurtin, Generalized Ginzburg-Landau and Cahn-Hilliard equations based on a microforce balance, Physica D 92 (1994) 178–192.

[57] P. Neff, A finite-strain elastic-plastic cosserat theory for polycrystals with grain rotations, Int. J. Eng. Sci. 44 (2006) 574–594. doi:10.1016/j.ijengsci.2006.04.002.

[58] R. Hardin, N. Sloane, McLaren's improved snub cube and other new spherical designs in three dimensions, Discrete Comput. Geom. 15 (1996) 429–441.

[59] A. Grillo, R. Prohl, G. Wittum, A generalised algorithm for anelastic processes in elastoplasticity and biomechanics, Math. Mech. Solids 22(3) (2017) 502–527. doi:10.1177/1081286515598661.

[60] X. Bi, G. Li, S. Doty, N. Camacho, A novel method for determination of collagen orientation in cartilage by Fourier transform infrared imaging spectroscopy (FT-IRIS), Osteoarthr. Cartil. 13 (2005) 1050–1058.

[61] W. Ehlers, B. Markert, Inverse poroelasticity as a fundamental mechanism in biomechanics and mechanobiology, Nat. Commun. 1002(8) (2017) 1–10. doi:10.1038/s41467-017-00801-3.

[62] G. Capriz, Continua with Microstructure. Springer Tracts in Natural Philosophy, vol. 35, Springer, New York, 1989.

[63] S. Quiligotti, G. Maugin, F. dell'Isola, An eshelbian approach to the nonlinear mechanics of constrained solid-fluid mixtures, Acta Mech. 160 (2003) 45–60. doi:10.1007/s00707-002-0968-z.